



This is a peer-reviewed, post-print (final draft post-refereeing) version of the following published document and is licensed under All Rights Reserved license:

Matthews, John A., Wilson, Peter, Winkler, Stefan, Mourné, Richard W., Hill, Jennifer L. ORCID logo
<https://orcid.org/0000-0002-0682-783X>, Owen, Geraint, Hiemstra, John F., Hallang, Helen and Geary, Andrew P. (2019) Age and development of active cryoplanation terraces in the alpine permafrost zone at Svartkampan, Jotunheimen, southern Norway. Quaternary Research, 92 (3). pp. 641-664. doi:10.1017/qua.2019.41

Official URL: <http://dx.doi.org/10.1017/qua.2019.41>

DOI: <http://dx.doi.org/10.1017/qua.2019.41>

EPrint URI: <https://eprints.glos.ac.uk/id/eprint/7810>

Disclaimer

The University of Gloucestershire has obtained warranties from all depositors as to their title in the material deposited and as to their right to deposit such material.

The University of Gloucestershire makes no representation or warranties of commercial utility, title, or fitness for a particular purpose or any other warranty, express or implied in respect of any material deposited.

The University of Gloucestershire makes no representation that the use of the materials will not infringe any patent, copyright, trademark or other property or proprietary rights.

The University of Gloucestershire accepts no liability for any infringement of intellectual property rights in any material deposited but will remove such material from public view pending investigation in the event of an allegation of any such infringement.

PLEASE SCROLL DOWN FOR TEXT.

Age and development of active cryoplanation terraces in the alpine permafrost zone at Svartkampan, Jotunheimen, southern Norway

John A. Matthews, Peter Wilson, Stefan Winkler, Richard W. Mourné, Jennifer L. Hill, Geraint Owen, John F. Hiemstra, Helen Hallang and Andrew P. Geary

Abstract

Schmidt-hammer exposure-age dating (SHD) of boulders on cryoplanation terrace treads and associated bedrock cliff faces revealed Holocene ages ranging from 0 ± 825 to 8890 ± 1185 yr. The cliffs were significantly younger than the inner treads, which tended to be younger than the outer treads. Radiocarbon dates from the regolith of 3854 to 4821 cal yr BP (2σ range) indicated maximum rates of cliff recession of ~ 0.1 mm/year, which suggests the onset of terrace formation prior to the last glacial maximum. Age, angularity and size of clasts, together with planation across bedrock structures and the seepage of groundwater from the cliff foot, all support a process-based conceptual model of cryoplanation terrace development in which frost weathering leads to parallel cliff recession and hence terrace extension. The availability of groundwater during autumn freeze-back is viewed as critical for frost wedging and/or the growth of segregation ice during prolonged winter frost penetration. Permafrost promotes cryoplanation by providing an impermeable frost table beneath the active layer, focusing groundwater flow, and supplying water for sediment transport by solifluction across the tread. Snowbeds are considered an effect rather than a cause of cryoplanation terraces and cryoplanation is seen as distinct from nivation.

Keywords

cryoplanation terraces, Schmidt-hammer exposure-age dating, mountain permafrost, periglacial processes, alpine landform development, frost weathering, nivation.

Introduction

Cryoplanation terraces (also known as altiplanation or goletz terraces and by several other terms) are periglacial landforms consisting of nearly horizontal bedrock surfaces or benches, backed by frost-weathered bedrock cliffs (Demek, 1969a; Washburn, 1979; Ballantyne, 2018; French, 2018; Harris et al., 2018). The terraces are typically tens of metres wide and hundreds of metres long, with a thin cover of regolith. They may occur singly or as an altitudinal sequence of hillslope ‘steps’ that sometimes culminate in ‘summit flats’ (Czudek, 1995; Lauriol et al., 2006; Křížek, 2007; Hall and André, 2010; Nelson and Nyland, 2017).

Cryoplanation terraces are generally supposed to have developed by processes of ‘cryoplanation’ – commonly interpreted to include a combination of frost weathering on bedrock cliffs and the removal of the weathered debris by solifluction and/or flowing water – resulting in cliff recession and terrace extension (Boch and Krasnov, 1943; Demek, 1969b; Priesnitz, 1988; Lauriol, 1990; Ballantyne, 2018). Indeed, Schunke (1977) suggested that cryoplanation terraces may be the only meso-scale landforms that can be used to characterise the periglacial zone, and hence define a truly periglacial environment. The processes of cryoplanation also underpin attempts to define distinctive models of periglacial hillslope and landscape evolution (cf. Peltier, 1950; Richter et al., 1963; French, 2016).

However, although cryoplanation terraces have been widely recognised in regions with present or former non-glacial cold climates, such as Siberia (Boch and Krasnov, 1943; Demek, 1968; Czudek, 1995), Mongolia (Richter et al., 1963); Alaska (Reger and Péwé, 1976; Nelson, 1998; Nelson and Nyland, 2017), Northern Canada (Lauriol and Godbout, 1988; Lauriol et al., 2006), Central Europe (Demek, 1969a; Traczyk and Migon, 2000; Křížek, 2007), Iceland (Schunke and Heckendorff, 1976; Schunke, 1977), the Andes (Grosso and Corte, 1991), Antarctica (Hall, 1997; Hall and André, 2010) and the British Isles (Te Punga, 1956; Waters, 1962), criteria for the recognition of active features are largely lacking. In the absence of dating evidence, moreover, most examples discussed in the literature are of unknown age and many are regarded as relict. Furthermore, there is disagreement over the necessary climatic conditions under which cryoplanation terraces can form, and whether cryoplanation terraces are characteristic of permafrost environments, as advocated by Reger and Pewe (1976) or can also form under climatic regimes characterised only by seasonal frost (Demek, 1969a).

The precise processes constituting cryoplanation, the rate of development of cryoplanation terraces, their status as palaeoclimatic indicators, and their role in the evolution of periglacial landscapes, all remain highly controversial topics. Furthermore, as cryoplanation terraces are often the sites of long-lasting snowbeds, this has led to the suggestion that cryoplanation is essentially similar to ‘nivation’ – the suite of weathering and transport processes that may be enhanced by the presence of late-lying or perennial snow – which is another problematic subject (St-Onge, 1964, 1969; Hall, 1998; Thorn and Hall, 2002; Margold et al., 2011; Rixhon and Demoulin, 2013). Arguably, despite the recent research from the Antarctic, there has been little progress in understanding cryoplanation terraces since the definitive monograph of Demek (1969a): new insights are therefore long overdue.

This paper presents the results of an investigation of active cryoplanation terraces recently discovered at Svartkampan in the permafrost zone of NE Jotunheimen, alpine southern Norway. These landforms are believed to be the first active cryoplanation terraces to be recognised as such in Norway and have the potential to resolve several of the aforementioned controversies regarding the nature and significance of cryoplanation and related topics. Our specific objectives are as follows:

1. To describe the morphology of the proposed cryoplanation terraces.
2. To date the terraces using Schmidt-hammer exposure-age dating (SHD), complemented by radiocarbon dating, and hence provide firm evidence of landform age and present levels of activity.
3. To assess observational evidence of the environmental controls on terrace formation at the site, including geological structure, climate, permafrost, snow, and groundwater hydrology.
4. To test current ideas on cryoplanation processes in the light of the new evidence from Svartkampan, and propose a process-based conceptual model of cryoplanation terrace development.

Location and environment

Svartkampan is a spur located on the northern slope of the Galdhøpiggen massif of northeastern Jotunheimen, the highest mountains in Norway (Figure 1). The cryoplanation terraces (sites 1-10) occur as a series of north-facing steps with backing cliffs cut into bedrock at an altitude of 1540-1575 m above sea level (Figures 1c and 2a). These terraces sit on the northern rim of Juvflye, a high-altitude plateau, where related forms have been mapped as perennial snowbeds but not as cryoplanation terraces (Ødegård et al., 1987). The study sites lie at least 500 m above the tree line: close to the upper altitudinal limit of the mid-alpine belt, which occurs locally at ~1600 m (Matthews et al., 2018a; see also, NIJOS, 1991). Extensive areas of active and relict periglacial patterned ground (sorted circles, garlands and stripes) characterise the largely till-covered landscape at and above the altitude of the sites (Ødegård et al., 1987, 1988; Winkler et al., 2016) where bedrock outcrops are relatively rare. Beneath the bedrock cliffs, the treads of the cryoplanation terraces have a similar surface cover of regolith with an extensive pavement of boulders and cobbles, disturbed soils and a sparse vegetation cover (Figure 2b).

Most of the study area is composed of pyroxene-granulite gneiss (Lutro and Tveten, 1996) but the location of the terraces coincides with a shear zone within the gneiss. Observations from the backing cliffs of the terraces show that this zone consists mainly of alternating flaggy layers of varied lithologies including fine-grained black to dark green mylonite and coarser-grained grey, sheared gneiss. Both lithologies have lozenge-shaped rotated feldspar crystals and larger pods (>5 cm) of relatively unshaped but rotated gneiss. Also present are rounded feldspar crystals (typically 1-2 cm), which give a ‘pebbly’ appearance resembling augen gneiss, white quartz-feldspar layers (possibly pre-deformational), and occasional larger intrusions of peridotite, which weathers to a distinctive orange-brown colour. Although not very common at the main terrace (sites 1-8) and the upper terraces (sites 9 and 10), the ‘pebbly’ gneiss predominates at another prominent terrace located below and to the north-west of the main terrace at 1525 m a.s.l.

Mean annual air temperature (MAAT) estimated from boreholes near the study site at 1560 m a.s.l., where permafrost is present, is -2°C with a mean July air temperature of $+5^{\circ}\text{C}$ and a mean January air temperature

of $-8\text{ }^{\circ}\text{C}$ (Farbrot et al., 2011; Lilleøren et al., 2012). These temperature data are consistent with the earlier estimate of $-2.6\text{ }^{\circ}\text{C}$ for MAAT at 1500 m a.s.l. interpolated from MAAT measurements at 11 meteorological stations around Jotunheimen (Ødegård et al., 1992). Annual snow depth is 1.0-1.5 m (www.se.norge.no/), while mean annual precipitation (MAP) is 800-1000 mm (Isaksen et al., 2011) with a late-summer maximum characteristic of the continental climatic regime of eastern Norway. However, strong winds on Juvflye result in comparatively little snow cover and a late maximum snow depth of only 0.5 m in May (Ødegård et al., 1992); our study sites in a leeward position will accumulate significantly higher values than this.

Permafrost is widespread in this area of Jotunheimen, where the lower limit of discontinuous permafrost lies at ~ 1450 m a.s.l. (Ødegård et al., 1996; Isaksen et al., 2002; Harris, et al. 2009; Farbrot et al., 2011) and active-layer thickness may be up to 5 m at 1600 m a.s.l. (Hipp et al., 2014). However, the lower limit of permafrost in alpine rock walls in the area is highly dependent on aspect and is likely to descend to at least 1300 m a.s.l. where these face north (Hipp et al., 2014), possibly within the range 1250-1400 m a.s.l. (Steiger et al., 2016). There can be no doubt, therefore, that the bedrock cliffs characterising the cryoplanation terraces at Svartkampan are underlain by permafrost. Permafrost is likely to have existed throughout the Holocene at altitudes >1600 m a.s.l. in the study area (Lilleøren et al., 2012). At the slightly lower altitude of the study sites, therefore, permafrost could have been absent during the Holocene thermal maximum of the early Holocene, although it may well have survived in the north-facing bedrock cliffs. The lowest permafrost limits of the Holocene seem to have occurred during the ‘Little Ice Age’ (Lilleøren et al., 2012), when MAAT was $\sim 1.0\text{ }^{\circ}\text{C}$ lower than in AD 1960-1990 (Nesje et al., 2008).

At the maximum of the last (Weichselian) glaciation, the highest areas of Jotunheimen were located close to the main ice divide and ice accumulation area of the Scandinavian ice sheet. Deglaciation is considered to have occurred in the early Holocene by 9.7 ka, following the Preboreal Erdalen event (cf. Dahl et al., 2002; Matthews and Dresser, 2008). This conventional interpretation is consistent with basal radiocarbon dates obtained from peat bogs and lakes from the valleys surrounding the Galdhøpiggen massif (Barnett et al., 2000; Nesje and Dahl, 2001; Matthews et al., 2005, 2018b; Hormes et al., 2009), empirical evidence of deglaciation elsewhere in southern Norway and broad-scale reconstruction of the Scandinavian ice-sheet deglaciation (Goehring et al., 2008; Nesje, 2009; Mangerud et al., 2011; Hughes et al., 2016; Stroeven et al., 2016; Marr et al., 2018).

Methodology

Observations and measurements were made at 10 sites on three cryoplanation terraces (Figures 1c and 3). Cross-profiles of the terrace tread and backing cliff were measured at each site to define the overall terrace morphology, using a 30-m tape and Abney level between breaks of slope. Two excavations were made in the tread of the main terrace (where the boulder cover was least extensive) to examine the subsurface, particularly the bedrock profile beneath the regolith cover. At each site, a total of 300 Schmidt-hammer R-values were measured, including: 100 boulders each from the inner and outer halves of the tread (one impact per boulder), and a sample of 100 impacts from the backing cliff (impacts widely spaced across the cliff face). A mechanical N-type Schmidt hammer (Proceq, 2004) was used throughout and periodically tested on the manufacturer’s test anvil to ensure no deterioration in performance following a large number of impacts (cf. McCarroll, 1987, 1994). Schmidt-hammer measurements were restricted to boulders or bedrock of the dominant local lithology, namely mylonitised pyroxene-granulite gneiss. Unstable or small boulders were avoided, as were boulder or bedrock edges, joints or cracks, and lichen-covered or wet surfaces (cf. Shakesby et al., 2006; Viles et al., 2011; Matthews and Owen, 2016).

High-resolution, calibrated-age, Schmidt-hammer exposure-age dating (SHD) techniques followed the approach developed by Matthews and Owen, (2010), Matthews and Winkler (2011) and Matthews and McEwen (2013). The approach is based on establishing a local, linear calibration equation relating mean Schmidt-hammer R-value to rock-surface exposure age based on two surfaces of known age (‘old’ and ‘young’ control points). The control points used in this study relate to the local mylonitised pyroxene-granulite gneiss. The ‘old’ control point, which is located within 200 m of the western end of the main terrace (M in Figure 1c), consists of glacially-scoured bedrock surfaces. The age of 9.7 ka assigned to these surfaces is the conventional age of deglaciation in central Jotunheimen (Matthews et al., 2018b; see above). The surfaces are exposed in a small channel last occupied by meltwater during deglaciation, when water flowed north from three small lakes that currently drain towards the south-east (Figure 1c). The bedrock surface of the modern cliff at site 8 was used

as the young control point with an age of zero years. This is justified on two grounds. First, this cliff surface was lichen free when the R-values were measured, which indicates a surface age of <25 years based on various estimates of the time required for the establishment of crustose *Rhizocarpon* lichens in Jotunheimen (Matthews, 2005; Matthews and Vater, 2015). Second, R-values from this cliff surface are similar but slightly higher than those characterising angular boulders located about 100 m from the Vesle-Juvbreen glacier snout on terrain that, according to aerial photographic evidence, has an estimated age of 50 years (Matthews et al., 2014).

The resulting Schmidt-hammer exposure ages are derived with 95% confidence intervals (Ct) that depend on the error associated with the calibration equation (Cc) and the error of the surface to be dated (Cs). This particular approach to SHD has been successfully applied to many different types of landforms composed of coarse rock particles and/or bedrock in southern Norway and elsewhere, including raised beaches (Shakesby et al., 2011), rock glaciers (Matthews et al., 2013), moraines (Matthews et al., 2014), pronival ramparts (Matthews and Wilson, 2015), snow-avalanche impact landforms (Matthews et al., 2015), periglacial patterned ground (Winkler et al., 2016), blockfields (Wilson and Matthews, 2016; Marr et al., 2018); blockstreams (Wilson et al., 2017) and rock-slope failures (Matthews et al., 2018b).

SHD was complemented by AMS radiocarbon dating of soil material within the regolith that overlies the bedrock beneath the terrace tread. The dated material constitutes a disturbed Humic Regosol (Ellis, 1979). Dating was carried out on bulk samples following acid wash pretreatment by Beta Analytic Inc using the INTCAL13 database (Reimer et al., 2013) and Bayesian probability analysis (Bronk Ramsey, 2009).

Organic content and particle size were measured for samples of soil and sub-soil. Weight loss-on-ignition at 550 °C (Heiri et al., 2001) was determined for samples dried at 105 °C. Particle size analysis involved sieving and further analysis of the <1 mm fraction by laser diffraction using a Mastersizer 2000 (Malvern Instruments Ltd, 2007; Mingard et al., 2009).

Clast roundness and size, and the proportion of *in situ* fractured clasts, were measured on the terrace treads and cliffs as a basis for inferring the possible origins of clasts and the effectiveness of frost weathering processes. Clast roundness was assessed for boulders and cobbles comprising the surface of the inner and outer parts of the tread separately at each site using a five-point roundness scale (Powers, 1953) and a sample size of 150 clasts. Comparable samples of clasts resting on cliff ledges were also examined. The size (longest visible axis) of the largest 25 clasts was recorded separately for angular (roundness classes: very angular and angular) and edge-rounded clasts (roundness classes: subangular, subrounded and rounded) on the terrace treads. The proportion of fractured clasts on each terrace tread was determined, based on a sample size of 200 clasts.

Structural geological measurements made of the bedrock cliff included horizontal and vertical joint spacing ($n = 25$): joints were defined as fractures or cracks >1 m long and >1 mm wide. The strike and dip of metamorphic layering in the cliff face were also measured using a compass clinometer for comparison with layering in the buried bedrock terrace revealed by excavation of the regolith cover.

Results

Terrace morphology

Morphology of the terraces is summarised by the cross-profiles from the 10 sites (Figure 4) and illustrated further by general views of selected sites (Figure 5). All profiles have a similar northerly aspect. Terrace treads are 7.0 – 22.0 m wide and backing cliffs are 1.5 – 6.0 m high. Slope angles of the treads and cliffs are 2–12 ° and 35–80 °, respectively, with a sharp break of slope or ‘knickpoint’ at the cliff base, sometimes resulting in an overhang (Figure 5c). No bedrock is visible at site 4, where a steep (30 °) boulder ‘ramp’ is assumed to bury a bedrock cliff. It should also be noted that the outer edge of the terraces at sites 5 and 6 terminate at low bedrock outcrops. At the other sites, the outer edge of the terrace tread is defined by a marked steepening of the slope. The height of the backing cliff is defined here conservatively as the relatively steep lowest part of the cliff, excluding the often degraded upper parts where there is a marked break of slope.

Clast characteristics on terrace treads and cliffs

Clasts on the inner part of the terrace tread (Table 1) are invariably more angular (combined angular and very angular clasts, 14-77 %) than those on the outer part (5-35 %). Furthermore, excluding site 4 (where the cliff is buried), the clasts on the cliffs are substantially more angular (49-97 %) than the clasts on the inner terrace treads. Although there is no trend in roundness or size of clasts along the length of the main terrace, site 8 has consistently higher proportions of angular clasts than any of the other sites on both the inner and outer treads and on the backing cliff. Angular clasts predominate on cliffs at most sites but it is only at site 8 where the proportion approaches 100 %. Elsewhere, there is a variable mixture of angular and edge-rounded clasts, the proportion of angular clasts reaching only 13 % on the boulder 'ramp' at site 4.

The size of the angular clasts on the treads tends to be larger (79-120 cm) than the size of the edge-rounded clasts (59-94 cm) with, in most cases, non-overlapping 95 % confidence intervals. The proportion of *in situ* fractured clasts (Figure 6a) on the treads is consistently low at all sites (3.1-12.8 %) with < 6 % at most sites.

Patterned ground on treads

Sorted circles (Figure 6b) up to 2 m in diameter occasionally occur individually or in small groups in the low-angle tread surfaces. Their fine centres are clearly recognisable, but the outer boundaries of the clast-rich borders are poorly defined against the clast-covered tread surface. Poorly-defined solifluction lobes also occur in a few places on the treads. However, most tread surfaces are characterised by a thin cover of angular and edge-rounded clasts forming a largely undifferentiated pavement of boulders and cobbles. Where present, patches of fines are generally vegetated with mid-alpine grass-heath and snowbed plant communities.

Subsurface bedrock, regolith and soil characteristics

The underlying bedrock terrace was located beneath 60-80 cm of regolith at the excavation between sites 5 and 6 (Figure 7). The regolith consists of a matrix-supported diamicton, the <2 mm fraction of which consists of 43-83 % sand, 16-49 % silt and 2-8 % clay (n = 6 samples). Median grain-sizes of all six samples (50-150 μm) are frost susceptible according to textural limits for frost-susceptible sediments (Beskow, 1935; Harris, 1981).

A well-developed Humic Regosol (Ellis, 1979, 1980) has developed in the uppermost part of the regolith. This soil is up to 45-cm thick and characterised by disturbed organic-rich, dark grey-brown layers and streaks (organic content 13.1-15.2 %) but no mineral horizon differentiation. With distance from the cliff base, the soil becomes lighter in colour and thinner and has more of the characteristics of an alpine Brown Soil (Ellis, 1979, 1980). Beneath the deepest organic-rich material, the lower part of the regolith (subsoil) has a much lower organic content (0.7-2.6 %), and an increasing density of rock fragments towards the underlying bedrock (see also Figure 6c).

The bedrock terrace at the base of the excavation (Figure 7) has a slope of 3°, which is comparable to the slope of the terrace tread at the site (5°). That the bedrock terrace is indeed *in situ* is confirmed by the strike and dip of 167° (range 154–188°; n = 3) and 22° NE (range 18–26°), which agree closely with the strike and dip in the exposed adjacent cliff of 138° (range 125–177°; n = 9) and 18° NE (range 10–26°). It should be noted that the second excavation failed to reach bedrock because of the presence of numerous large boulders throughout the regolith.

Joint spacing in cliffs

Vertical and horizontal joints occur frequently in the cliffs, commonly with an increase in density near the cliff base (Figure 6d). The spacing of both vertical and horizontal joints is very variable, ranging from a few centimetres to 185 cm with no systematic pattern discernible between sites. Mean vertical and horizontal joint spacing (with 95 % confidence intervals) for all sites is 50 ± 10 and 26 ± 2 cm, respectively; the closer spacing of horizontal joints reflecting the greater density of joints parallel to metamorphic layering, as seen in Figure 6d.

Seepage water at the cliff/tread junction

Water was observed seeping from joints at the base of the cliff at several sites despite former snowbeds having melted away earlier in the summer (Figure 8). The soil at the site of both excavations was damp, saturated with water in several places, and one of the trenches was slowly filling with water in late July 2018, despite the sites having experienced a severe drought for at least a month before these observations were made. Furthermore, a dry drainage channel crossed the tread of the terrace at site 2 beneath which the sound of flowing water could be heard, possibly indicative of piping.

R-values from terrace treads and cliffs

R-values for cliffs vary consistently along the length of the main terrace from a mean value of 42.59 ± 2.26 at site 1 to 59.66 ± 1.24 at site 8 (Table 2). The 95 % confidence intervals demonstrate, moreover, that this spatial variation along the main terrace is highly statistically significant. Cliff sites from the upper terraces (sites 9 and 10) exhibit intermediate values. The R-value distributions (Figure 9) consolidate these results and show highly variable, multimodal, negatively skewed and/or relatively broad platykurtic distributions indicative of mixed-age populations and hence diachronous surfaces (Matthews et al., 2014, 2015; Winkler et al., 2016; Marr et al., 2018). Only cliff site 8 exhibits the low-variability, unimodal, symmetrical distribution of R-values that is expected for a surface of uniform age. There is also a strong inverse relationship for cliff sites between R-value variability (as reflected in standard deviation values and confidence intervals) and mean R-values, which is consistent with an increase in variability as the extent of chemical weathering of the rock surfaces and the increase in mean rock surface age results in decreasing R-values (Aydin and Basu, 2005; Matthews et al, 2013, 2016).

Mean R-values from inner terrace treads at sites 2-8 are, in most cases, significantly lower than those from the corresponding cliffs by up to 7 units, and mean R-values from outer terrace treads tend to be even lower, though not significantly lower than those from the inner treads (Table 2). These patterns suggest that the mixed-age boulder populations on the inner terraces are older than those on the bedrock cliffs and that the boulder populations on the outer terraces are even older. Furthermore, the long tails that characterise most of the R-value distributions in Figure 9 are clearly the result of the relatively old component of mixed-age populations. Apart from site 1, all the outer tread sites have mean R-values within the relatively narrow range of 43.19-47.47 and are therefore relatively old compared with the inner tread and cliff sites. Mean R-values from both the inner and outer treads at site 1 are, however, significantly higher than those of the corresponding cliff, which is not consistent with the results from the other sites and requires further explanation (see discussion below). At the upper terraces (sites 9 and 10), mean R-values from the terrace treads do not differ significantly from those of their cliffs and again exhibit intermediate values compared with the sites from the main terrace.

Control point R-values and calibration equation

R-values characterising potential control point surfaces from the local area (Table 3) include data from the mylonitised pyroxene-granulite gneiss surfaces used to derive the SHD calibration equation and calibration curve for this study (Figure 10). These data are close to but differ slightly from those relating to non-mylonitised pyroxene-granulite gneiss obtained in this study (G1 and G2 in Figure 1c and Table 3) and available from previous work (G3, from Matthews et al., 2014). Broad confidence intervals of the order of 1.0 R-value units reflect the variability of the local bedrock and suggest that R-values may be relatively high on recently exposed mylonite surfaces.

Although the 'old' control point derived from mylonite has yielded intermediate R-values with respect to non-mylonitised surfaces of the same known age, it nevertheless represents the best available for obtaining calibrated ages for the cryoplanation terraces. The fact that the mean R-value of the mylonitised 'young' control-point surface exceeds that of non-mylonitised boulders recently exposed on the Vesl Juvbreen glacier foreland (Matthews et al., 2014) supports our use of the cliff surface as a modern control surface. Furthermore, the percentage frequency distributions of R-values for both control points (Figure 11) exhibit symmetrical

distributions with no reason to doubt they are representative of single-age surfaces. It is particularly noteworthy that the distribution for the 'old' control point lacks the low R-values and negatively skewed distributions that are characteristic features of most of the terrace treads and cliffs.

SHD ages

The consistent decrease in SHD age of the cliffs along the length of the main terrace from 8890 ± 1185 yr at site 1 to 0 ± 825 yr at site 8 clearly shows spatial variation in exposure age from west to east (Table 4 and Figure 12). Indeed, there is a statistically significant linear relationship ($r = 0.96$; $p < 0.001$) between SHD age and distance from site 1 (Figure 13).

With the exception of site 1, confidence intervals show that the inner treads on the main terrace are consistently older than the cliffs, and there is a clear decrease in SHD age from sites 4 (7610 ± 1210 yr) through 8 (2605 ± 1000 yr), all of which have inner terraces that are significantly older than their cliffs. Although the linear relationship between SHD age and distance along the inner terrace is only marginally statistically significant when data from all eight sites are included ($r = 0.65$; $p < 0.10$; Figure 13), there is considerable improvement in the strength of this relationship ($r = 0.80$; $p < 0.05$) if anomalous site 1 is omitted. The overlap in the confidence intervals for cliffs and inner treads at sites 2 and 3 indicate, however, little evidence of a significant difference in age. Also, again with the exception of site 1, the SHD ages of outer treads tend to be older than the inner treads but the age difference is relatively small and statistically significant only at sites 7 and 8 (Figure 12). Thus, in general, terrace treads are older than their corresponding cliffs, and outer treads are the oldest parts of the terraces, the SHD ages of which range from 4690 ± 1025 yr at site 1 to 8575 ± 1270 yr at site 4. However, there is little evidence of any systematic variation in SHD age within the outer treads.

The upper terraces exhibit little variation in SHD age between the two sites or between cliffs and treads. With all ages between 5940 ± 1040 yr and 7855 ± 1130 yr, the exposure ages of the upper terraces are clearly intermediate between those of the youngest and oldest parts of the main terrace.

The anomalous pattern exhibited by site 1, where the cliff has a very much older exposure age than both the inner and outer treads (the SHD ages of which do not differ significantly from each other) is difficult to explain. Disturbance of the terrace tread by frost heave and frost sorting, bringing relatively unweathered boulders to the ground surface, provides a possible explanation.

¹⁴C ages

Two radiocarbon dates from two sides of the same trench, sampled at a distance of 50-60 cm from the cliff base, yielded a calibrated age between 3854 and 4821 cal yr BP at the 2σ range (Table 5 and Figure 7). This age estimate represents the maximum age of the overlying sedimentary material of the tread and a minimum age for the underlying bedrock platform at the sample point. The single date from the second excavation, sampled at a distance of 30 cm from the cliff, yielded the somewhat younger age estimate of 3345-3084 cal yr BP.

Discussion

Recognising cryoplanation terraces

Cryoplanation terraces are problematic largely because their recognition and characterisation are based almost entirely on morphological evidence. There is a tendency, moreover, to attribute all bench-like landforms on hillslopes in periglacial environments to cryoplanation (Ballantyne, 2018). Furthermore, most examples referred to in the literature appear to be relict and it has even been suggested that some such terraces are not characteristic of a periglacial environment at all, may be pre-Quaternary in age and/or may simply reflect geological structure (Büdel, 1982; French, 2016, 2018). Although this study is heavily reliant on morphological evidence, an advantage of the cryoplanation terraces at Svartkampan is that they are currently active, at least in part. We are confident, therefore, that the combination of morphological evidence with dating evidence, field observations

relevant to structure and process, and the general climatic characteristics of the sites, provides a firm basis for attributing their origin to cryoplanation.

Dating cryoplanation terraces

There have been few previous attempts to date cryoplanation terraces, none of which has had much success. Vague generalisations have resulted from relative-age dating based on morphostratigraphy, weathering-rind thickness, vegetation or lichen cover (Péwé, 1970; Reger, 1975; Lauriol et al., 1997; Nelson, 1998). However, it has been concluded that they probably develop over very long periods of time, which supports similar ideas based on the observation that they are well developed in terrain that has never been glaciated or was not glaciated during the last glaciation (Reger and Péwé, 1976; Lauriol and Godbout, 1988; Nelson and Nyland, 2017). To the authors' knowledge, the results of numerical-age dating techniques have been presented in two published papers only (Creameens et al., 2005; Lauriol et al., 2006): the first applied ^{36}Cl cosmogenic-nuclide exposure-age dating to two possible cryoplanation summit flats; the second obtained nine ^{14}C dates from the regolith cover of the treads of undoubted cryoplanation terraces.

In the present study we have used two numerical-age dating techniques in the context of cryoplanation terraces for the first time, including the first application of SHD. Comparable results have been achieved from the extensive use of SHD on bedrock exposed in the backing cliffs and on the boulder cover of treads; and these results are in turn compatible with the ^{14}C dating of organic sediments buried beneath the surface of treads. The SHD ages provide evidence of the extent to which the terraces are currently active, while the ^{14}C ages provide estimates of maximum rates of cliff recession and terrace extension during the late Holocene. However, neither approach yields close estimates of landform age defined as the period of time over which the cryoplanation terraces formed.

SHD ages and current activity

For a diachronous surface, SHD age estimates the average exposure-age of the sampled surface (Matthews et al., 2014, 2015; Winkler et al., 2016). The bedrock and boulder surfaces sampled from the cryoplanation terraces in this study vary considerably in their average exposure age (Table 4; Figure 12). Only the bedrock cliff sampled at site 8, with an SHD age of zero, is representative of a uniformly modern, active surface. All the other surfaces represent mixed-age populations, with increasing levels of activity and decreasing exposure-age and current activity along the length of the main terrace from west to east (sites 1 to 8). The remarkable linear SHD age and hence activity gradient exhibited by the cliffs (Figure 13) shows not only that the cliffs at the eastern end of the main terrace are the most active but also that those at the western end are essentially relict. Indeed, the SHD age of the cliff at site 1 (8890 ± 1185 yr) indicates very little activity except <1000 yr after deglaciation.

The pattern of SHD ages between the cliffs, inner treads and outer treads, which is most apparent towards the eastern end of the main terrace (sites 5 to 8), is also enlightening (Figure 12). The fact that the inner tread is significantly older than the cliff at these sites, and that the outer tread is even older (significantly so at sites 7 and 8), points to the cliffs being the source of the relatively fresh boulders in the treads. These relatively fresh boulders, having been added to an older boulder population, would have reduced the average exposure-age of the surface boulders of the tread. This interpretation of the ages is supported by the clast roundness analyses, which demonstrate that the proportion of angular clasts in the cliffs is higher than on the treads and that the proportion on the inner treads tends to be higher than on the outer treads. Thus, the greater proportion of weathered clasts on the treads gives rise to the older SHD ages.

In theory, frost disturbance may reduce the exposure-age of clasts on the treads. Frost heave and frost sorting have the potential to bring relatively unweathered clasts to the surface, and frost fracturing of clasts embedded in the tread may expose fresh, unweathered rock surfaces. However, as the observed pattern of SHD ages (i.e. inner treads are older than cliffs and outer treads are characterised by the oldest ages) is the opposite of what would be the expected outcome of these disturbances, none of these disturbances are likely to have had an appreciable effect on the SHD ages (except, perhaps, at site 1).

Rate of terrace formation and landform age

The radiocarbon dates of ~3000, 4000 and 5000 cal yr BP for organic material at the base of the humic regosol at distances of 30, 50 and 60 cm, respectively, from the bedrock cliff (Table 5 and Figure 7) provide maximum estimates for the rate of bedrock cliff recession and terrace extension of ~0.10, 0.125 and 0.12 mm per year, respectively. These values are comparable to the measured rockwall recession rates compiled from a wide range of lithologies in arctic and alpine periglacial environments (Murton, 2013; Ballantyne, 2018; French, 2018).

Given that the deglaciation of Svartkampan occurred 9700 years ago, maximum cliff recession rates of the order of 0.1 mm per year are insufficient for the cryoplanation terraces to have been eroded entirely within the Holocene. Indeed, extrapolation of this rate implies that at least 56–176 ka would be required to erode the terraces, the widths of which range from 7–22 m. We conclude, therefore, that the onset of terrace formation is likely to have occurred prior to the last (Weichselian) glacial maximum, in periods with a periglacial climate. Subsequent survival of terraces also seems likely, which would have been possible under a relatively thin, cold-based ice sheet (cf. Kleman, 1994; Hättestrand and Stroeven, 2002; Juliussen and Humlum, 2007; Marr et al., 2018).

It must be acknowledged, however, that the inference of a wholly periglacial origin for the terraces depends on several assumptions, namely: (1) our estimated maximum rate of cliff recession is representative for the late Holocene; (2) similar rates can be applied to the entire Holocene and also to pre-Holocene periglacial regimes; and (3) alternative processes (such as differential subglacial erosion) did not contribute to these landforms. The third assumption may not be reasonable, given the nature of the regolith that covers the bedrock surface of the treads. It is apparent that much of the regolith consists of a diamicton, with numerous edge-rounded clasts and abundant fine matrix. Similar edge-rounded clasts occur on the cliffs and completely bury the cliff at site 4. Both the diamicton and the edge-rounded clasts most likely originated as till, deposited during deglaciation and subsequently reworked by periglacial mass wasting. It is not unrealistic to suggest, therefore, that subglacial erosion through plucking contributed to preparation and erosion of the cliff prior to the Holocene and hence could account for a substantial share of the present-day width of the terraces.

Frost-weathering processes on the cliffs

Frost weathering is conventionally regarded as the primary process in explaining the backwearing of cliffs in the context of cryoplanation terraces (Boch and Krasnov, 1943, Demek, 1969a; 1969b; Priesnitz, 1988; Czudek, 1995). However, the sparsity of direct process studies has been universally recognised as a major problem in their interpretation. Nevertheless, several lines of indirect evidence from Svartkampan point strongly to the main process being the production of relatively large rock fragments by frost wedging (alternatively termed macrogelivation) as a result of the freezing of water in pre-existing cracks) (Murton, 2013; Ballantyne, 2018).

First, the modern cliff at site 8 and active parts of cliffs at the other sites are clearly the main source of the clasts littering the inner treads of the terraces. These well-jointed cliffs (frost-riven cliffs to use the term commonly employed in cryoplanation research) produce clasts that match those on the inner treads in terms of exposure-age, angularity and size. The low proportions of *in situ* fractured clasts on the treads indicates, moreover, that comminution of existing clasts is not a feasible alternative source for abundant, large angular clasts on the treads (cf. Berrisford, 1991).

Second, abundant moisture is available at the base of the cliffs from groundwater, which originates from permafrost thaw and summer rainfall as well as snowmelt. Water is as essential as sub-zero temperatures for frost weathering (Hall et al., 2002; Thorn and Hall, 2002; Thorn et al., 2011). It remains available at the Svartkampan sites during freeze-back, enabling ice to form in pre-existing joints and cracks. Frost wedging is most likely to occur at this time in response not only to the volumetric expansion of ice in the cracks but also to the growth of segregation ice as water migrates towards a freezing front that is penetrating deep into the cliff (cf. Walder and Hallet, 1985; Matthews et al., 1986; Hallet et al., 1991; Murton et al., 2006; Matsuoka and Murton, 2008). Although the development of segregation ice has been investigated and discussed largely in relation to porous rocks, it would also be expected in association with interconnected microcracks in the layered mylonitised gneiss at Svartkampan. Significantly, cryoplanation terraces and other frost-riven cliffs in the Sudetes Mountains (Central Europe) appear to be preferentially associated with gneissic and schistose bedrock (Traczyk

and Migon, 2000).

Third, evidence for fractured bedrock and *in situ*, loosely-attached rock fragments forming breccia, is particularly abundant close to the foot of the cliff, both above (Figure 6d) and below (Figure 6c) the surface of the tread. This is precisely where groundwater seepage occurs, and hence where most water is available for ice formation in cracks, and where frost weathering would be expected to undercut the cliff, producing the sharp cliff/tread junction and maintaining the terrace cross-profile shape. Maximum seepage at the cliff base is attributed to the topography of the ground surface, combined with high joint density and the configuration of the still-frozen substrate.

Fourth, both cliff and buried bedrock surfaces (Figure 7) cut across bedrock structures, effectively excluding an explanation based purely on geology. In the absence of evidence for alternative processes capable of producing flights of such terraces, this has generally been accepted as strong evidence for cliff recession as a result of frost weathering, provided debris removal by mass wasting is sufficient to prevent the accumulation of debris at the cliff base (Demek, 1969a, Presnitz, 1988; Czudek, 1995; Nelson and Nyland, 2017).

Transport processes on the treads

Transport of sediments across the treads of cryoplanation terraces is commonly attributed to solifluction and flowing water, with gelifluction, frost creep, slopewash, sheet wash, snow meltwater, suprapermafrost meltwater, infiltration water, subsurface flow, piping, and suffosion, all having been mentioned in the literature (Demek, 1969a; Czudek and Demek, 1971; Reger and Péwé, 1975; Presnitz, 1988; Lauriol, 1990; Czudek, 1995). Solifluction and various types of water flow occur at Svartkampan, but the observational and dating evidence presented above indicate that such transport must have been extremely slow throughout the Holocene. Although supranival transport cannot be ruled out as a contributory process, the coarser material could not have been moved by most of the water-flow processes. Furthermore, many of the edge-rounded surface clasts and most of the silty-sand matrix comprising the regolith seem to have originated as till, which was deposited during deglaciation. Subsequently, the frost-susceptible regolith was disturbed by solifluction but, according to our dating, it was transported no more than a few metres across the terraces during the Holocene.

Solution (Rapp, 1960; Lauriol et al., 1997; Thorn et al., 2011) and wind transport (Demek, 1969a; Lauriol et al., 1997; Lamirande et al., 1999) probably contributed to the removal of some fines from the regolith at some places and times, but these processes cannot have had a major effect on the overall volume and fabric of the regolith over the Holocene timescale. Similarly, cryoturbation and frost sorting undoubtedly contributed to disturbance of the frost-susceptible regolith, and may well have favoured infiltration, the concentration of surface and subsurface water flow and piping (Presnitz, 1988) while leaving the bulk of the regolith intact.

Developmental model of cryoplanation terraces

Various seasonal processes contribute to the development of active cryoplanation terraces at Svartkampan. The presence of groundwater near the cliff base during autumn and early winter freeze-back is of critical importance (Figure 14a). At this time, groundwater is moving downslope under gravity along cracks and joints within the active layer of the cliff and emerging near the base of the cliff where the groundwater table intersects the ground surface. Permafrost and/or infiltration of rainwater must be the major water source as, by this time, the late-lying snowbeds have melted away. Also, groundwater in the active layer cannot penetrate the permafrost, which is acting as an aquiclude, or at least an aquitard (Woo, 2012; Liao and Zhuang, 2017). Thus, above the permafrost table, and especially at the cliff base, groundwater is available for ice wedging and/or the growth of segregation ice during refreezing of the active layer.

Transportation of debris across the terrace tread takes place mainly during the spring and early summer, when thaw consolidation leads to solifluction and snow meltwater is abundant (Figure 14b). Also in spring and summer, melting of ice in the cliff is likely to trigger rockfall onto the terrace tread, either directly or indirectly via the snowbed surviving at that time on the inner tread. However, rates of solifluction are very slow due to the low gradient of the tread and the outer tread tends to be more stable than the inner tread, affected less by solifluction and perhaps more by cryoturbation and frost sorting. Beneath the regolith-covered inner terrace tread,

the active layer is likely to be thinner than beneath the bedrock cliff, because of its higher ice content and consequent greater amount of latent heat required to thaw the ground. In addition, the active layer will tend to be thinner under the snowbed due to the insulating properties of late-lying snow. Conditions are different on the tread during freeze-back: the snowbed has melted away, surface sediments are drier, and the reduced availability of water leads to relatively low rates of bedrock frost weathering beneath the tread.

Over the long-term, the zone of maximum frost weathering close to the cliff base leads to the cliff being undercut, and to parallel retreat of a near-vertical cliff (Figure 14c). This model bears some similarity to that originally proposed by Boch and Krasnov (1943), namely enhanced frost weathering towards the cliff base, comparatively little lowering of the bedrock beneath the terrace tread, parallel retreat of the cliff over time, and solifluction as the main process evacuating sediment across the tread. However, several important new features of our model should be highlighted, particularly: (1) *undercutting* of the cliff by frost weathering at the cliff-tread junction, which produces and maintains a *near-vertical* cliff; (2) provision of a *groundwater-based mechanism* for cliff recession; (3) *seasonal dimensions* to both cliff recession and sediment evacuation from the tread; and (4) *negligible* lowering over time of the near-horizontal bedrock surface beneath the tread, attributed to the thermal properties of the regolith cover, leading to a relatively thin active layer, which may not penetrate far into the bedrock.

Structural control of terrace initiation?

As with earlier models that more-or-less require an initial cliff-like form, our model does not provide an explanation for the initiation of cryoplanation terrace development. Without an appropriate pre-existing landform, it is difficult to see how enhanced frost-weathering would produce such a cliff on a land surface with a uniform slope angle. Possible precursors (proto-cliffs) might be controlled by geological structure and/or accentuated by selective glacial erosion at times when a Pleistocene ice-sheet was not cold-based and protective. Dilatation joints and exfoliation following repeated glacial loading and unloading might also be considered but, ultimately, no definite answer can be given. From their alignment and location, at least some form of structural control of a proto-cliff seems likely (though subsequent cliff retreat does not follow the smaller-scale bedrock structures).

Permafrost promotes cryoplanation

Reger and Péwé (1976) argued strongly that cryoplanation requires permafrost, and it seems to be accepted that the most favourable conditions occur where permafrost is present under relatively continental climates (Crudek, 1995; Hall, 1998; Nelson and Nyland, 2017). Our research at Svartkampan indicates that permafrost is an important water source for frost weathering and solifluction, and that an impermeable permafrost table confines meltwater flow to the active layer, contributes to the focusing of frost weathering towards the cliff base, and provides a 'base level' below which frost weathering is ineffective. Apparently active cryoplanation terraces have nevertheless been described from areas with deep seasonal ground freezing, such as low-alpine zones and maritime polar regions (Demek 1969a; Schunke and Heckendorff, 1976; Crudek 1995). In view of slow rates of development, however, it is difficult to establish whether such terraces experienced seasonal freezing throughout their development. Thus, we conclude that although permafrost promotes cryoplanation it cannot yet be said to be a necessary condition.

Cryoplanation is not the same as nivation

It has been suggested that there are similarities in the morphology and genesis of cryoplanation terraces and nivation benches or hollows (Margold et al., 2011; Ballantyne, 2018), and that cryoplanation and nivation can be conceptualised as representing different parts of a single process spectrum (Hall, 1998; Thorn and Hall, 2002). An important insight following from our research on the Svartkampan terraces, however, is that snow, and processes of nivation, play only a secondary role in cryoplanation and the formation of cryoplanation terraces. This is in agreement with the proposal of Hall (1998) and Thorn and Hall (2002) that cryoplanation is

associated with relatively cold climates, permafrost and snow-free conditions, whereas nivation is characterised by the presence of snow in milder and wetter climates. Thus, we propose that cryoplanation should be regarded as essentially distinct from nivation.

The characteristic process of cryoplanation and our model of cryoplanation terrace development is frost weathering at the cliff base: this leads, over time, to the parallel retreat of the cliff and terrace extension (Figure 14c). Thermal insulation by snow dampens the annual freeze-thaw cycle rather than accentuates it (Draebing et al., 2017) and, most importantly, snow is normally no longer available as a moisture source during freeze-back. Water for ice-growth at this time comes from groundwater – supra-permafrost meltwater flow and infiltration water from autumn rainfall – rather than snowbeds. Thus, any late snowbeds on the terrace treads (see, for example Figure 2) are an effect rather than a cause of the cryoplanation terrace and, more likely than not, slow down the rate of cliff recession and terrace extension. Interestingly, the original definition of nivation (Matthes, 1900) did not include frost weathering of bedrock.

Processes of nivation (snow-generated processes capable of enhancing geomorphic work) (cf. Thorn, 1976, 1988; Thorn and Hall, 1980, 2002; Nyberg, 1991; Christiansen, 1998a, 1998b) do contribute to the transport of material across the terrace tread. During spring and summer thaw, solifluction occurs beneath and in front of snowbeds on the tread, and snow meltwater transports fine sediments away from the cliff while rockfall material from the cliff may undergo supranival transport (Figure 14a). However, the dates obtained on both organic sediments and surface boulders in this study demonstrate extremely slow Holocene transport rates with relatively small quantities of material being transported for a short distance across the inner terrace tread, which leaves the outer tread in an essentially relict state.

Summary and conclusions

We have dated cryoplanation terraces for the first time using two different dating techniques and present a process-based conceptual model of cryoplanation terrace development. SHD was applied to surface boulders on terrace treads and bedrock cliffs and ^{14}C dating was applied to organic-rich sediment within the regolith on the tread. This chronological information, combined with observational evidence, has enabled several controversial aspects of cryoplanation to be addressed.

The statistically significant decrease in SHD mean age ($\pm 95\%$ confidence interval) of the cliffs along the length of the main terrace, from 8890 ± 1185 yr at site 1 to 0 ± 825 yr at site 8, demonstrates significant spatial variation in exposure age and activity. This strong west-east age gradient seems to reflect subtle topographic variations with consequent effects on groundwater hydrology and frost weathering. With the exception of site 1, the inner treads on the main terrace yielded consistently older SHD ages than the cliffs, and the SHD ages of outer treads tend to be older than the inner treads. None of the SHD ages are older than the Holocene but most terraces have active and relict elements. The SHD ages are complemented by three ^{14}C dates of between 3854 and 4821 cal yr BP (2σ range), which indicate a maximum rate of cliff recession of the order of 0.1 mm per year. Extrapolation of this rate suggests that the terraces began to form before the last glacial maximum, survived glaciation beneath cold-based ice, and resumed active development in the Holocene.

Excavation has demonstrated that the terraces cut across bedrock structures yet most of the regolith on the terrace treads is interpreted as diamicton derived from till deposited during deglaciation and subsequently reworked by solifluction and cryoturbation. Boulder pavement caps much of the regolith on the inner treads and the pavement tends to be formed of angular boulders derived from the cliffs; whereas on the outer treads, edge-rounded clasts are characteristic. The age, angularity and size of clasts on the inner treads supports frost-weathering as the primary process leading to cliff recession and terrace extension. During autumn freeze-back, snowbeds have melted yet seepage water is still available at the cliff-base, where effective frost wedging and/or the growth of segregation ice in joints and cracks is inferred to occur during prolonged winter frost penetration. Thus, the availability of groundwater during freeze-back is considered to be critical for cryoplanation, which proceeds slowly by parallel retreat of a cliff undercut by frost weathering.

Permafrost seems to promote the formation of well-developed cryoplanation terraces by providing an impermeable frost table beneath the active layer, focusing groundwater flow towards the cliff base, and supplying water during spring and summer thaw. Together with snowmelt, supra-permafrost meltwater promotes the transport of regolith across the terrace surface, especially by solifluction following thaw

consolidation. However, such transport processes are very slow under the relatively continental climatic conditions of northeastern Jotunheimen. It is argued that seasonal frost is less likely to promote cryoplanation and terrace development.

Contrary to the view expressed in several recent publications, our results suggest that cryoplanation should be seen as different from nivation. Snow appears to play, at most, only a secondary role in cryoplanation. And enhanced frost weathering linked to groundwater hydrology during freeze-back, which is so important for cryoplanation, does not constitute a nivational process.

Acknowledgements

Fieldwork was carried out on the Swansea University Jotunheimen Research Expeditions, 2017 and 2018. We thank Anika Donner for assistance in the field, Charles Harris for discussions on the possible effects of permafrost, named (Martin Margold and Atle Nesje) and unnamed reviewers for comments leading to improvement of the manuscript, Ole Jakob and Tove Grindvold for logistical support, and Anna Ratcliffe for drawing up the figures for publication. This paper constitutes Jotunheimen Research Expeditions Contribution No. 207 (see: <http://jotunheimenresearch.wixsite.com/home>)

References

- Aydin, A., Basu, A., 2005. The Schmidt hammer in rockmaterial characterisation. *Engineering Geology* 81, 1-14.
- Ballantyne, C.K., 2018. *Periglacial Geomorphology*. Wiley-Blackwell: Chichester.
- Barnett, C., Dumayne-Peaty, L., Matthews, J. A., 2000. Holocene climatic change and tree-line response in Leirdalen, central Jotunheimen. *Review of Palaeobotany and Palynology* 117, 119–137.
- Berrisford, M.S., 1991. Evidence for enhanced mechanical weathering associated with 855 seasonally late-lying and perennial snow patches, Jotunheimen, Norway. *Permafrost and Periglacial Processes* 2, 331-340.
- Beskow, G., 1935. Tjälbildningen och tjällyftningen med särskild hänsyn till vägar och järnvägar. Sveriges Geologiske Undersökning, Series C 375, Årbok 26, 1-242.
- Boch, S.G., Krasnov, I.I., 1943. On altoplanation terraces and ancient surfaces of levelling in the Urals and associated problems. In: Evans, D.J.A. (Ed.), (1994) *Cold Climate Landforms*. Wiley, Chichester, pp. 177-186. [Translated from Russian]
- Bronk Ramsey, C., 2009. Bayesian analysis of radiocarbon dates. *Radiocarbon* 51, 337-360.
- Büdel, J. 1981. *Klima- Geomorphologie, 2nd edition*. Bornträger, Berlin-Stuttgart.
- Christiansen, H.H., 1998a. Nivation forms and processes in unconsolidated sediments, NE Greenland. *Earth Surface Processes and Landforms* 23, 751-760.
- Christiansen, H.H., 1998b. 'Little Ice Age' nivation activity in northeast Greenland. *The Holocene* 8, 719-728.
- Creameans, D.L., Darmody, R.G., George, S.E., 2005. Upper slope landforms and age of bedrock exposures in the St. Francois Mountains, Missouri: a comparison of relict periglacial features in the Appalachian Plateau of West Virginia. *Geomorphology* 70, 71-84.
- Czudek, T., 1995. Cryoplanation terraces – a brief review and some remarks. *Geografiska Annaler Series A (Physical Geography)* 77A, 95-105.
- Czudek, T., Demek, J., 1971. Pleistocene cryoplanation in the Česká Vpocina highlands, Czechoslovakia. *Transactions of the Institute of British Geographers* 52, 95-112.
- Dahl, S.O., Nesje, A., Lie, Ø., Fordheim, K., Matthews, J.A., 2002. Timing, equilibrium-line altitudes and climatic implications of two early-Holocene readvances during the Erdalen Event at Jostedalbreen, western Norway. *The Holocene* 12, 17-25.
- Demek, J., 1968. Cryoplanation terraces in Yakutia. *Biuletyn Peryglacjalny* 17, 91-116.
- Demek J., 1969a. Cryoplanation terraces, their geographical distribution, genesis and development. *Rozprawy Československé Akademie Věd, Rada Matematických a Přírodních Věd Rocnik* 79(4): 80pp.
- Demek, J., 1969b. Cryogene processes and the development of cryoplanation terraces. *Biuletyn Peryglacjalny* 18, 115-125.
- Draebing, D., Haberkorn, A., Krautblatter, M., Kenner, R., Phillips, M. 2017. Thermal and mechanical responses resulting from spatial and temporal snow cover variability in permafrost rock slopes, Steintaelli, Swiss Alps. *Permafrost and Periglacial Processes* 28, 140-157.
- Ellis, S., 1979. The identification of some Norwegian mountain soil types. *Norsk Geografisk Tidsskrift* 33, 205-212.
- Ellis, S., 1980. Soil-environmental relationships in the Okstindan Mountains, north Norway. *Norsk Geografisk Tidsskrift* 34, 167-176.

- Farbrot, H., Hipp, T.F., Etzelmüller, B., Isaksen, K., Ødegård, R.S., Schuler, T.V., Humlum, O., 2011. Air and ground temperature variations observed along elevation and continentality gradients in southern Norway. *Permafrost and Periglacial Processes* 22, 343–360.
- French, H.M., 2016. Do periglacial landforms exist? A discussion of the upland landscapes of northern interior Yukon, Canada. *Permafrost and Periglacial Processes* 27, 219–228.
- French, H.M., 2018. *The Periglacial Environment, 4th edition*. Wiley-Blackwell: Chichester.
- Goehring, B. M., Brook, E. J., Linge, H., Raisbeck, G. M., Yiou, F., 2008. Beryllium-10 exposure ages of erratic boulders in southern Norway and implications for the history of the Fennoscandian Ice Sheet. *Quaternary Science Reviews* 27, 320–336.
- Grosso, S.A., Corte, A.E., 1991. Cryoplanation surfaces in the Central Andes at latitude 35° S. *Permafrost and Periglacial Processes* 2, 49–58.
- Hall, K., 1997. Observations on “cryoplanation” benches in Antarctica. *Antarctic Science* 9, 181–187.
- Hall, K., 1998. Nivation or cryoplanation: different terms, same features? *Polar Geography* 22, 1–16.
- Hall, K., André, M.-F., 2010. Some further observations regarding “cryoplanation terraces” on Alexander Island. *Antarctic Science* 22, 175–183.
- Hall, K., Thorn, C.E., Matsuoka, N., Prick, A., 2002. Weathering in cold regions: some thoughts and perspectives. *Progress in Physical Geography* 26, 577–603.
- Hallet, B., Walder, J.S., Stubbs, C.W., 1991. Weathering by segregation ice growth in microcracks at sustained sub-zero temperatures: verification from an experimental study using acoustic emission. *Permafrost and Periglacial Processes* 2, 283–300.
- Harris, C., 1981. *Periglacial Mass Wasting: a Review of Research*. Geobooks, Norwich [British Geomorphological Research Group Research Monograph 4].
- Harris, C., Arenson, L.U., Christiansen, H.H., Etzelmüller, B., Frauenfelder, R., Gruber, S., Haeberli, W., Hauck, C., Hoelzle, M., Humlum, O., Isaksen, K., Käab, A., Kern-Luetschg, M.A., Lehning, M., Matsuoka, N., Murton, J.B., Noezli, J., Phillips, M., Ross, N., Seppälä, M., Springman, S.M., Vonder Mühll, D.V., 2009. Permafrost and climate in Europe: monitoring and modelling thermal, geomorphological and geotechnical responses. *Earth Science Reviews* 92, 117–171.
- Harris, S.A., Brouchkov, A., Cheng G., 2018. *Geocryology: Characteristics and Use of Frozen Ground and Periglacial Landforms*. CRC Press-Balkema: Leiden.
- Hättestrand, C., Stroeve, A.P., 2002. A relict landscape in the centre of the Fennoscandian glaciation: geomorphological evidence of minimal Quaternary glacial erosion. *Geomorphology* 44, 127–143.
- Heiri, O., Lotter, A.F., Lemcke, G., 2001. Loss on ignition as a method for estimating organic and carbonate content in sediments: reproducibility and comparability of results. *Journal of Paleolimnology* 25, 101–110.
- Hipp, T., Etzelmüller, B., Westermann, S., 2014. Permafrost in alpine rock faces from Jotunheimen and Hurrungane, southern Norway. *Permafrost and Periglacial Processes* 25, 1–13.
- Hormes, A., Blaauw, M., Dahl, S.-O., Nesje, A., Possnert, G., 2009. Radiocarbon wiggle-match dating of proglacial lake sediments – implications for the 8.2 ka event. *Quaternary Geochronology* 4, 267–277.
- Hughes, A. L. C., Gyllencreutz, R., Lohne, Ø., Mangerud, J., Svendsen, J. L., 2016. The last Eurasian ice sheets – a chronological database and time-slice reconstruction, DATED-1. *Boreas* 45, 1–45.
- Isaksen, K., Hauck, C., Gudevang, E., Ødegård, R.S., Sollid, J.L., 2002. Mountain permafrost distribution in Dovrefjell and Jotunheimen, southern Norway, based on BTS and DC resistivity tomography data. *Norsk Geografisk Tidsskrift* 56, 122–136.
- Isaksen, K., Ødegård, R.S., Etzelmüller, B., Hilbich, C., Hauck, C., Farbrot, H., Eiken, T., Hagen, J.O., Hipp, T.F., 2011. Degraded mountain permafrost in southern Norway: spatial and temporal variability of ground temperatures, 1999–2009. *Permafrost and Periglacial Processes* 22, 361–377.
- Juliussen, H., Humlum, O., 2007. Preservation of blockfields beneath Pleistocene ice sheets on Solen and Elgahogna, central-eastern Norway. *Zeitschrift für Geomorphologie N.F. 51, Supplementband 2*, 113–138.
- Kleman, J., 1994. Preservation of landforms under ice sheets and ice caps. *Geomorphology* 9, 19–32.
- Křížek, M., 2007. Periglacial landforms above the alpine timberline in the High Sudetes. In Goudie, A.S and Kalvoda, J. (eds) *Geomorphological Variations*, 313–337. P3K Publishing, Prague.
- Lamirande, I., Lauriol, B., Lalonde, A.E., Clark, I.D., 1999. La production de limon sur tes terrasses de cryoplanation dans les Monts Richardson, Canada. *Canadian Journal of Earth Sciences* 36, 1645–1654. et al., 1999
- Lauriol, B., 1990. Cryoplanation terraces, northern Yukon. *Canadian Geographer* 34, 347–351.
- Lauriol, B., Godbout, L., 1988. Les terrasses de cryoplanation dans le nord du Yukon: distribution, genèse et âge. *Geographie Physique et Quaternaire* 42, 303–314.
- Lauriol, B.M., Lalonde, A.E., Dewez, V., 1997. Weathering of quartzite on a cryoplanation terrace in northern Yukon. *Permafrost and Periglacial Processes* 8, 147–153.
- Lauriol, B., Lamirande, I., Lalonde, A.E., 2006. The Giant Steps of Bug Creek, Richardson Mountains, N.W.T., Canada. *Permafrost and Periglacial Processes* 17, 267–275.
- Liao, C., Zuang, Z., 2017. Quantifying the role of permafrost distribution in groundwater and surface water interactions using a three-dimensional hydrological model. *Arctic, Antarctic and Alpine Research* 49, 81–100.

- Lilleøren, K.S., Etzelmüller, B., Schuler, T.V., Ginås, K., Humlum, O., 2012. The relative age of permafrost – estimation of Holocene permafrost limits in Norway. *Global and Planetary Change* 92–Lutro, O., Tveten, E., 1996. *Geologiske kart over Norge, berggrunnskart Årdal, 1:250,000*. Norges Geologiske Undersøkelse, Trondheim.
- Malvern Instruments Ltd., 2007. *Mastersizer 2000, User Manual. MAN0384, Issue 1.0*.
- Mangerud, J., Gyllencreutz, R., Lohne, Ø., Svendsen, J.I., 2011. Glacial history of Norway. In: Ehlers, J., Gibbard, P.L., Hughes, P.D. (Eds.), *Quaternary Glaciations – Extent and Chronology: a Closer Look*. Elsevier, Amsterdam, pp. 279–298.
- Margold, M., Treml, V., Petr, L., Nyplová, P., 2011. Snowpatch hollows and pronival ramparts in the Krkonose Mountains, Czech Republic: distribution, morphology and chronology of formation. *Geografiska Annaler Series A (Physical Geography)* 93A, 137–150.
- Marr, P., Winkler, S., Löffler, J., 2018. Investigations on blockfields and related landforms at Blåhø (Southern Norway) using Schmidt hammer exposure-age dating: palaeoclimatic and morphodynamic implications. *Geografiska Annaler Series A (Physical Geography)* 100A, 285–306.
- Matthes, F.E., 1900. Glacial sculpture of the Bighorn Mountains, Wyoming. *United States Geological Survey 21st Annual Report 1899–1900*, 167–190.
- Matthews, J.A., 2005. ‘Little Ice Age’ glacier variations in Jotunheimen, southern Norway.: a study in regionally-controlled lichenometric dating of recessional moraines with implications for climate and lichen growth rates. *The Holocene* 15, 1–19.
- Matthews, J. A., McEwen, L. J., 2013. High-precision Schmidt hammer exposure-age dating (SHD) of flood berms, Vetlestølsdalen, alpine southern Norway: first application and some methodological issues. *Geografiska Annaler Series A, Physical Geography* 95, 185–194.
- Matthews, J. A., Owen, G., 2010. Schmidt-hammer exposure-age dating: developing linear age-calibration curves using Holocene bedrock surfaces from the Jotunheimen- Jostedalbreen regions of southern Norway. *Boreas* 39, 105–115.
- Matthews, J.A. and Vater, A.E., 2015. Pioneer zone geo-ecological change: observations from a chronosequence on the Storbreen glacier foreland, Jotunheimen, southern Norway. *Catena* 135, 219–230.
- Matthews, J. A., Wilson, P., 2015. Improved Schmidt-hammer exposure ages for active and relict pronival ramparts in southern Norway, and their palaeoenvironmental implications. *Geomorphology* 246, 7–21.
- Matthews, J. A., Winkler, S., 2011. Schmidt-hammer exposure-age dating (SHD): application to early Holocene moraines and a reappraisal of the reliability of terrestrial cosmogenic-nuclide dating (TCND) at Austanbotnbreen, Jotunheimen, Norway. *Boreas* 40, 256–270.
- Matthews, J.A., Dawson, A.G., Shakesby, R.A., 1986. Lake shoreline development, frost weathering and rock platform erosion in an alpine periglacial environment, Jotunheimen, southern Norway. *Boreas* 15, 33–50.
- Matthews, J. A., Berrisford, M.S., Dresser, P.Q., Nesje, A., Dahl, S.-O., Bjune, A. E., Bakke, J., Birks, H. J. B., Lie, Ø., Dumayne-Peaty, L., Barnett, C., 2005. Holocene glacier history of Bjørnbreen and climatic reconstruction in central Jotunheimen, southern Norway, based on proximal glaciofluvial stream-bank mires. *Quaternary Science Reviews* 24, 67–90.
- Matthews, J. A., Nesje, A., Linge, H., 2013. Relict talus-foot rock glaciers at Øyberget, upper Ottadalen, southern Norway: Schmidt hammer exposure ages and palaeoenvironmental implications. *Permafrost and Periglacial Processes* 24, 336–346.
- Matthews, J. A., Winkler, S., Wilson, P., 2014. Age and origin of ice-cored moraines in Jotunheimen and Breheimen, southern Norway: insights from Schmidt-hammer exposure-age dating. *Geografiska Annaler Series A, Physical Geography* 96, 531–548.
- Matthews, J.A., McEwen, L.J., Owen, G., 2015. Schmidt-hammer exposure-age dating (SHD) of snow-avalanche impact ramparts in southern Norway: approaches, results and implications for landform age, dynamics and development. *Earth Surface Processes and Landforms* 40, 1705–1718.
- Matthews, J. A., Owen, G., Winkler, S., Vater, A. E., Wilson, P., Mourne, R.W., Hill, J. L., 2016. A rock-surface microweathering index from Schmidt hammer R-values and its preliminary application to some common rock types in southern Norway. *Catena* 143, 35–44.
- Matthews, J.A., Hill, J.L., Winkler, S., Owen, G., Vater A.E., 2018a. Autosuccession in alpine vegetation: testing the concept on an altitudinal bioclimatic gradient, Jotunheimen, southern Norway. *Catena* 170, 169–182.
- Matthews, J.A., Winkler, S., Wilson, P., Tomkins, M.D., Dortch, J.M., Mourne, R.W., Hill, J.L., Owen, G., Vater, A.E., 2018b. Small rock-slope failures conditioned by Holocene permafrost degradation: a new approach and conceptual model based on Schmidt-hammer exposure-age dating, Jotunheimen, southern Norway. *Boreas* 47, 1144–1169.
- Matsuoka, N., Murton, J., 2008. Frost weathering: recent advances and future directions. *Permafrost and Periglacial Processes* 19, 195–210.
- McCarroll, D., 1987. The Schmidt hammer in geomorphology: five sources of instrument error. *British Geomorphological Research Group, Technical Bulletin* 36, 16–27.
- McCarroll, D., 1994. The Schmidt hammer as a measure of degree of rock surface weathering and terrain age. In: Beck, C. (Ed.), *Dating in Exposed and Surface Contexts*. University of New Mexico Press, Albuquerque, pp29–45.
- Mingard, K., Morrell, R., Jackson, P., Lawson, S., Patel, S., Buxton, R., 2009. Good Practice Guide for Improving the

- Consistency of Particle Size Measurement. National Physics Laboratory, Teddington [Measurement Good Practice Guide No. 111].
- Murton, J.B., 2013. Rock weathering. In: Elias, S.A. (Ed), *Encyclopedia of Quaternary Science, Volume 3*. Elsevier, Amsterdam, pp. 500-506.
- Murton, J.B., Peterson, R., Osouf, J.-C., 2006. Bedrock fracture by ice segregation in cold regions. *Science* 314, 1127-1129.
- Nelson, F.E., 1998. Cryoplanation terrace orientation in Alaska. *Geografiska Annaler Series A, Physical Geography* 71, 31-41.
- Nelson, F.E., Nyland, K.E., 2017. Periglacial cirque analogues: elevation trends of cryoplanation terraces in eastern Berigia. *Geomorphology* 293, 305-217.
- Nesje, A., 2009. Late Pleistocene and Holocene alpine glacier fluctuations in Scandinavia. *Quaternary Science Reviews* 28, 2119-2136.
- Nesje, A., Dahl, S.-O., 2001. The Greenland 8200 cal. yr BP event detected in loss- on-ignition profiles in Norwegian lacustrine sediment sequences. *Journal of Quaternary Science* 16, 155-166.
- Nesje, A., Dahl, S.O., Thun, T., Nordli, Ø., 2008. 'Little Ice Age' glacial expansion in western Scandinavia: summer temperature or winter precipitation? *Climate Dynamics* 30, 789-801.
- NIJOS, 1991. *Vegetasjonskart: Galdhøpiggen 1518 II (1:50,000)*. Norsk Institutt for Jord og Skogkartlegging (NIJOS), Ås
- Nyberg, R., 1991. Geomorphic processes at snowpatch sites in the Abisko Mountains, northern Sweden. *Zeitschrift für Geomorphologie N.F.* 35,321-343.
- Ødegård, R.S., Sollid, J.L., Liestøl, O., 1987. *Juvflya – Kvartærgeologi og geomorfologi MI:10.000*. Geografisk Institutt, Universitetet I Oslo, Oslo.
- Ødegård, R.S., Sollid, J.L., Liestøl, O., 1988. Periglacial forms related to terrain parameters in Jotunheimen, southern Norway. *Permafrost: V International Conference on Permafrost in Trondheim, Norway, August 1988, vol. 3*, Tapir, Trondheim, pp. 59-61.
- Ødegård, R.S., Sollid, J.L., Liestøl, O., 1992. Ground temperature measurements in mountain permafrost, Jotunheimen, southern Norway. *Permafrost and Periglacial Processes* 3, 231-234.
- Ødegård, R.S., Hoelzle, M., Johansen, K.V., Sollid, J.L., 1996. Permafrost mapping and prospecting in southern Norway. *Norsk Geografisk Tidsskrift* 50, 41-53.
- Peltier, L.C., 1950. The geographic cycle in periglacial regions as it relates to climatic geomorphology. *Annals of the Association of American Geographers* 40, 214-236.
- Péwé, T.L., 1970. Altiplanation terraces of early Quaternary age near Fairbanks, Alaska. *Acta Geographica Loziensia* 24, 357-363.
- Powers, M.C., 1953. A new roundness scale for sedimentary particles. *Journal of Sedimentary Petrology* 23, 117-119.
- Priesnitz, K., 1988. Cryoplanation. In: Clark, M.J. (Ed.), *Advances in Periglacial Geomorphology*. Wiley, Chichester, pp. 49-67.
- Proceq, 2004. *Operating instructions. Betonprüfhammer N/NR-L/LR*. Proceq SA, Schwerzenbach.
- Rapp, A., 1960. Recent development of mountain slopes in Karkevage and surroundings, northern Scandinavia. *Geografiska Annaler* 42, 65-200.
- Reger, R.D., 1975. Cryoplanation terraces of interior and western Alaska. PhD Thesis, Arizona State University, Tempe, Arizona.
- Reger, R.D., Péwé, T.L., 1976. Cryoplanation terraces: indicators of a permafrost environment. *Quaternary Research* 6, 99-109.
- Reimer, P.J., Bard, E., Bayliss, A., Beck, J.W., Blackwell, P.G., Bronk Ramsey, C., Buck, C.E., Cheng, H., Edwards, R.L., Friedrich, M., Grootes, P.M., Guilderson, T.P., Haflidason, H., Hajdas, I., Hatté, C., Heaton, T.J., Hoffmann, D.I., Hogg, A.G., Hughen, A.K., Kaiser, K.F., Kromer, B., Manning, S.W., Niu, M., Reimer, R.W., Richards, D.A., Scott, E.M., Southon, J.R., Staff, R.A., Turney, C.S.M., van der Plicht, A., 2013. INTCAL13 and MARINE13 radiocarbon age calibration curves 0- 50,000 years cal BP. *Radiocarbon* 55, 1869-1887.
- Richter, H., Haase, G., Barthel, H., 1963. Die Goleztterrassen. *Petermanns Geographische Mitteilungen* 107, 183-192.
- Rixhon, G., Demoulin, A., 2013. Evolution of slopes in a cold climate. In: Giardino, R., Harbor, J. (Eds), *Treatise on Geomorphology, Volume 8, Glacial and Periglacial Geomorphology*, 392-415. Academic Press: San Diego, CA.
- Schunke, E., 1977. Periglazialformen und formengesellschaften in der europäisch atlantischen Arktis und Subarktis. *Abhandlungen der Akademie der Wissenschaften in Göttingen, Mathematisch-Physicalische Klasse, Dritte Folge* 31, 39-62.
- Schunke, E., Heckendorff, W.D., 1976. Resistenzstufen und kryoplanation. Beobachtungen aus dem periglazialen Milieu Islands. *Zeitschrift für Geomorphologie. Supplement Band* 24, 88-98.
- Shakesby, R.A., Matthews, J.A., Owen, G., 2006. The Schmidt hammer as a relative- age dating tool and its potential for calibrated age dating in Holocene glaciated environments. *Quaternary Science Reviews* 25, 2846-2867.
- Shakesby, R.A., Matthews, J.A., Karlén, W., Los, S., 2011. The Schmidt hammer as a Holocene calibrated-age dating technique: testing the form of the R-value-age relationship and defining predicted errors. *The Holocene* 21, 615-628.
- Steiger, C., Etzelmüller, B., Westermann, S., Myhra, K.S., 2016. Modelling the permafrost distribution in steep rock

- walls in Norway. *Norwegian Journal of Geology* 96, 329-341.
- Stroeven, A. P., H attestrand, C., Kleman, J., Heyman, J., Fabel, D., Fredin, O., Goodfellow, B.W., Harbor, J. M., Jansen, J.D., Olsen, L., Caffee, M.W., Fink, D., Lundqvist, J., Rosqvist, G.C., Str mberg, B., Jansson, K. N., 2016: Deglaciation of Fennoscandia. *Quaternary Science Reviews* 147, 91–121.
- St-Onge, D.A., 1964. Les formes de nivation de L' le Ellef Ringnes, Territoires du Nord-Ouest. *Acta Geographica* 3, 287-304.
- St-Onge, D.A., 1969. Nivation landforms. *Geological Survey of Canada Paper* 69-30, 1-12.
- Te Punga, M.T., 1956. Altiplanation terraces in southern England. *Biuletyn Peryglacjalny* 4, 331-338.
- Thorn, C.E., 1976. Quantitative evaluation of nivation in the Colorado Front Range. *Geological Society of America Bulletin* 87, 1169-1178.
- Thorn, C.E., 1988. Nivation: a geomorphic chimera. In Clark, M.J. (ed.) *Advances in Periglacial Geomorphology*, 3-31. Wiley: Chichester.
- Thorn, C.E., Hall, K., 1980. Nivation: an arctic-alpine comparison and reappraisal. *Journal of Glaciology* 25, 109-124.
- Thorn C.E., Hall, K., 2002. Nivation and cryoplanation: the case for scrutiny and integration. *Progress in Physical Geography* 26, 533-550.
- Thorn, C.E., Darmody, R.G., Dixon, J.C., 2011. Rethinking weathering and pedogenesis in alpine periglacial regions: some Scandinavian evidence. In: Martini, I.P., French, H.M., P rez Albertini, A. (Eds) *Ice-marginal and periglacial processes and sediments*. Geological Society of London, Special Publications 354, pp. 183-193.
- Traczyk, A., Migon, P., 2000. Cold-climate landform patterns in the Sudetes. Effects of lithology, relief and glacial history. *Acta Universitatis Carolinae Geographica* 35 (Supplementum), 185-210.
- Viles, H., Goudie, A., Grabb, S., Lalley, J., 2011. The use of the Schmidt hammer and Equotip for rock hardness assessment in geomorphology and heritage science: a comparative analysis. *Earth Surface Processes and Landforms* 36, 320–333.
- Walder, J.S., Hallet, B., 1985. A theoretical model of the fracture of rock during freezing. *Bulletin of the Geological Society of America* 96, 336-346.
- Waters, R.S., 1962. Altiplanation terraces and slope development in Vest-Spitsbergen and south-west England. *Biuletyn Peryglacjalny* 11, 89-101.
- Washburn, A.L., 1979. *Geocryology: a Survey of Periglacial Processes and Environments*. Arnold, London.
- Wilson, P., Matthews, J.A., 2016. Age assessment and implications of late Quaternary periglacial and paraglacial landforms on Muckish Mountain, northwest Ireland, based on Schmidt-hammer exposure age dating (SHD). *Geomorphology* 270, 134–144.
- Wilson, P., Matthews, J.A., Mourn , R.W., 2017. Relict blockstreams at Insteheia, Valldalen-Tafjorden, southern Norway: their nature and Schmidt-hammer exposure age. *Permafrost and Periglacial Processes* 28, 286–297.
- Winkler, S., Matthews, J.A., Mourn , R.W., Wilson, P., 2016. Schmidt-hammer exposure ages from periglacial patterned ground (sorted circles) in Jotunheimen, Norway, and their interpretive problems. *Geografiska Annaler Series A, Physical Geography* 98, 265–285.
- Woo, M., 2012. *Permafrost Hydrology*. Springer, Heidelberg.

Figures

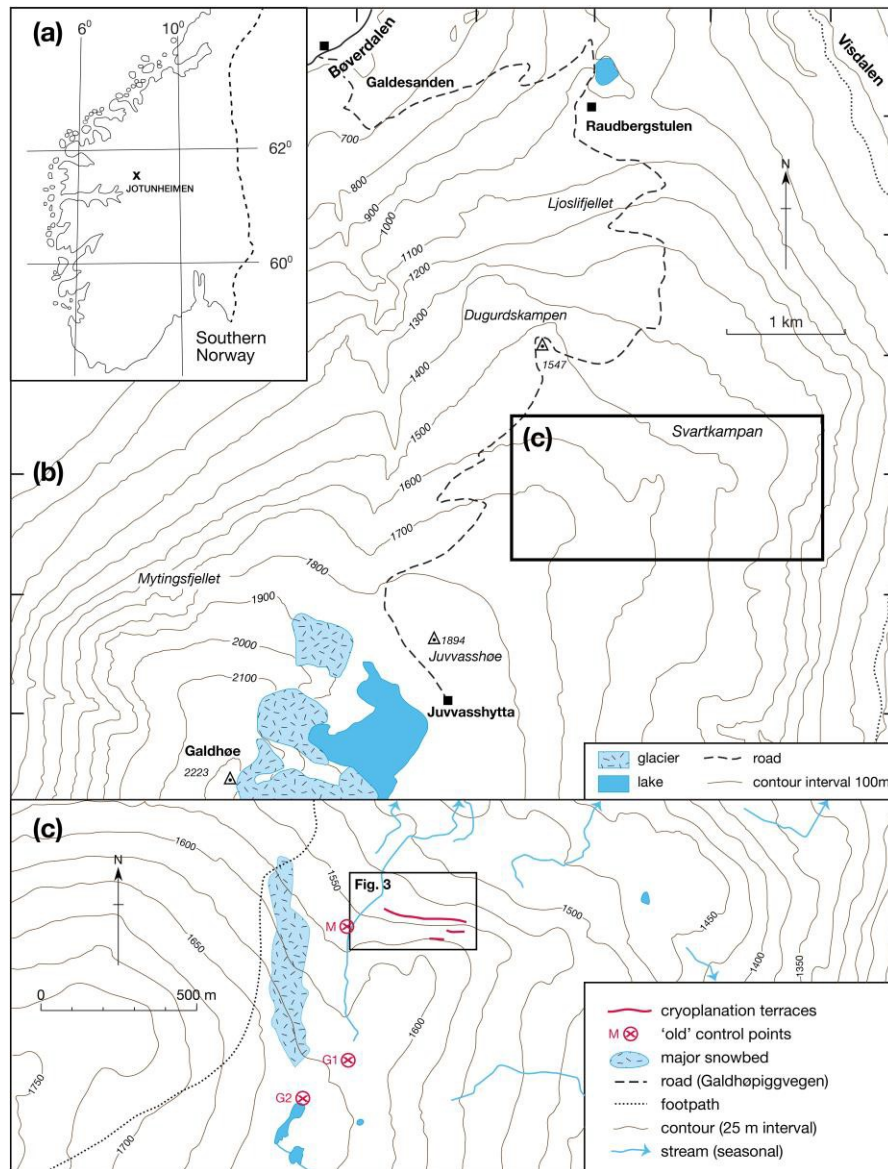


Figure 1. (a) Location of Jotunheimen, southern Norway; (b) location of Svartkampan, NE Jotunheimen; (c) location of the cryoplanation terraces at Svartkampan (source: <http://www.norgeskart.no>). Sites of control points for Schmidt-hammer exposure-age dating (M, G1 and G2; explained in the text) and location of Figure 3 are also shown.

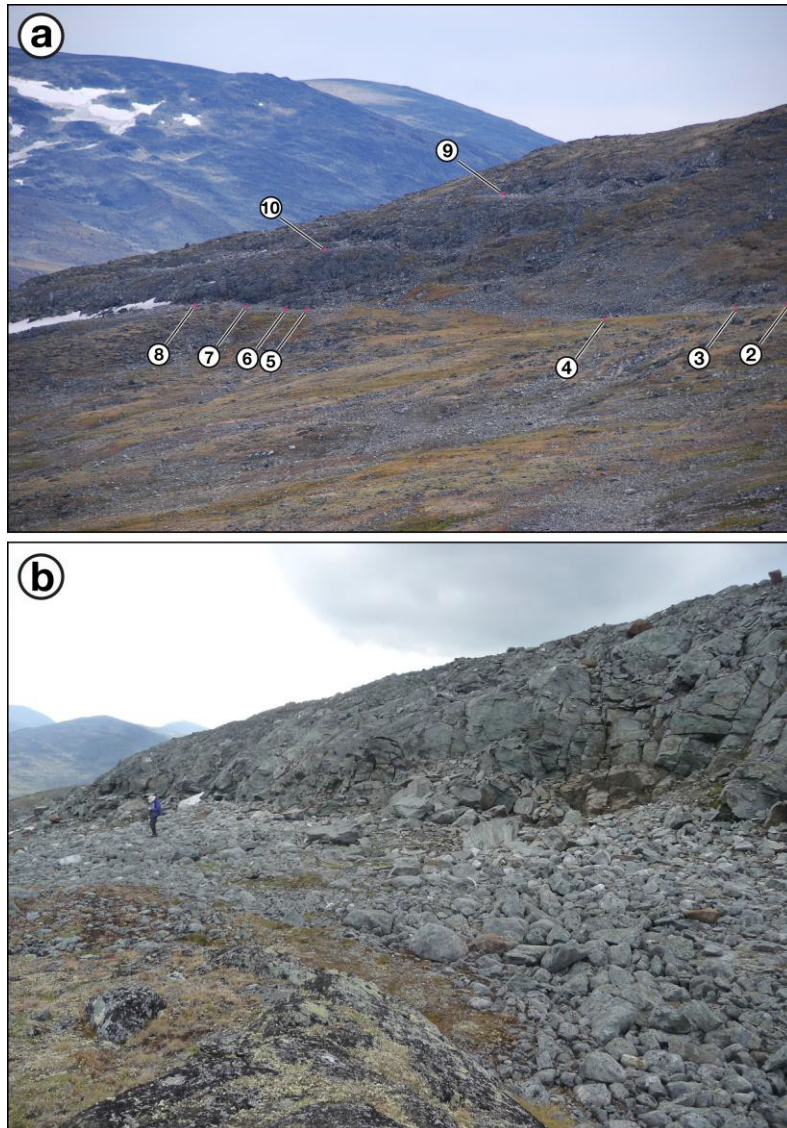


Figure 2. (a) The sequence of cryoplanation terraces at Svartkampan viewed from the north-west (23/07/2018). Numbers indicate the positions of cross-profiles and measurement sites 2-10. Note also the late-lying snowbed at the eastern end of the main terrace (to the left of site 8) and the near-absence of snow elsewhere on this terrace and on the two upper terraces (sites 9 and 10). (b) Detail of the eastern end of the main terrace (including sites 7 and 8; 22/07/2017). Note person for scale.

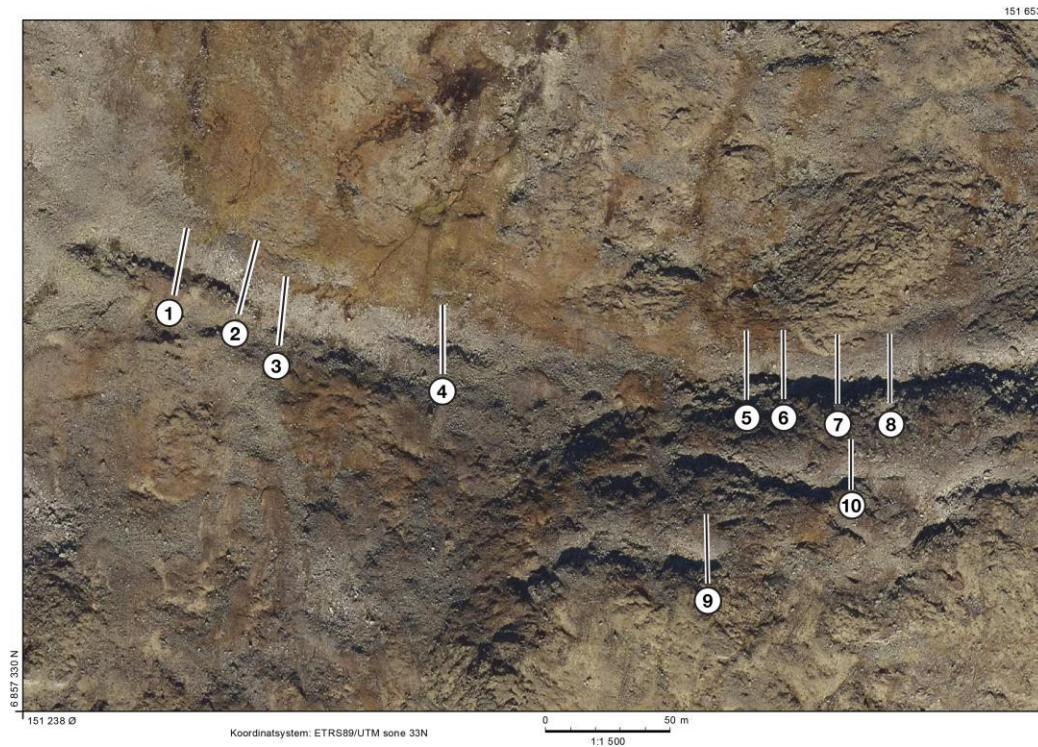


Figure 3. Vertical aerial photograph of the cryoplanation terraces flow on 25/09/2017 (source: <http://www.norgebilder.no>). Numbers indicate the positions of cross-profiles and measurement sites 1-10.

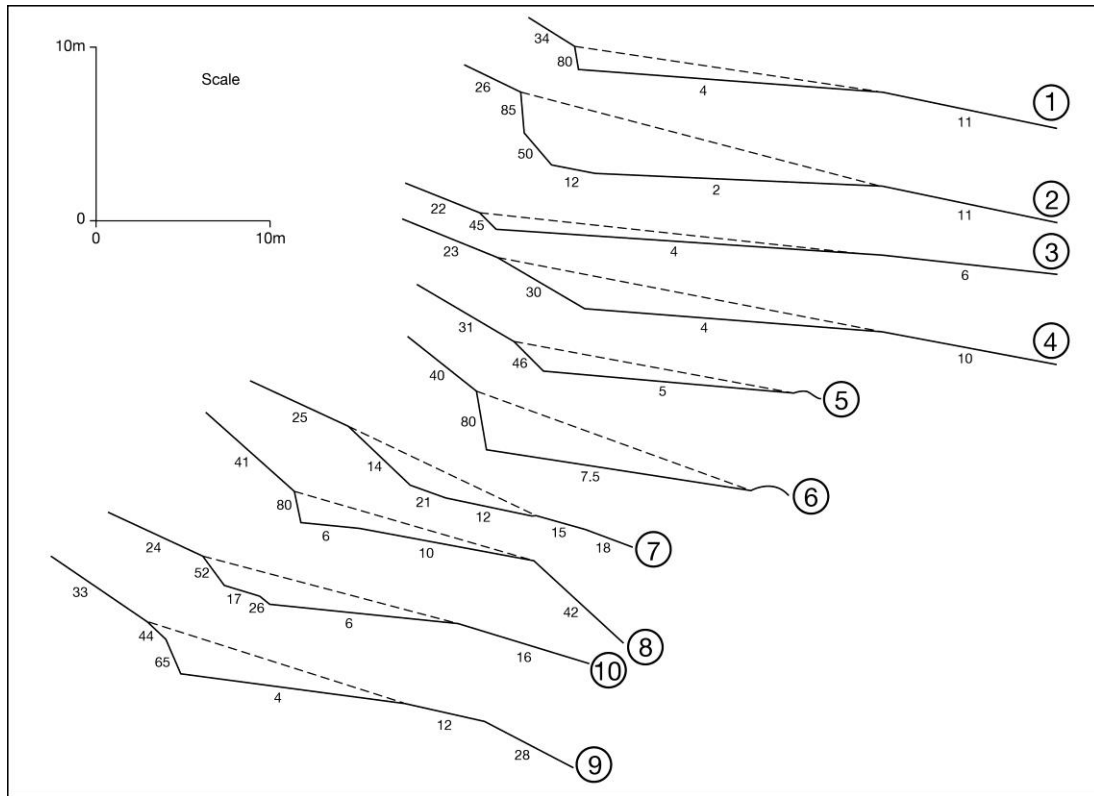


Figure 4. Cross-profiles of the cryoplanation terraces: sites 1-8 relate to the main terrace; sites 9 and 10 are on the upper terraces. Small numbers are slope angles of the slope segments (degrees). On each profile, the length of the terrace tread was halved to define the inner (closest to the cliff) and outer tread. Dashed lines suggest the volume of rock removed to form each terrace.

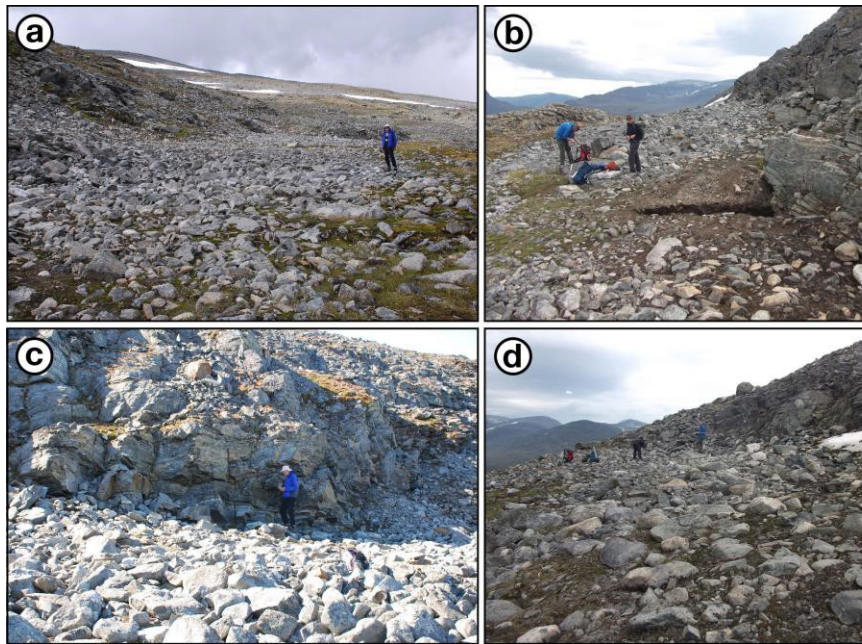


Figure 5. Photographs of selected cryoplanation terraces: (a) general view of sites 1-3 on the main terrace viewed from the east (30/07/2017); (b) general view of sites 6-8 on the main terrace from the north-west with excavation in the foreground (21/07/2018); (c) site 6 from the north (21/07/2017); (d) site 10 from the west (17/07/2018).

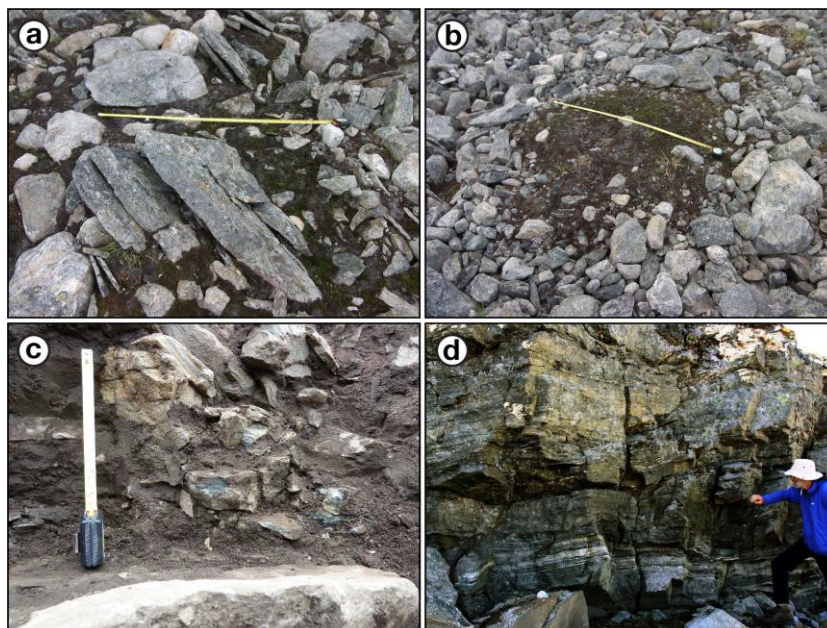


Figure 6. Details from cryoplanation terrace treads and cliffs: (a) sorted circle on the terrace tread at site 2 (scale length = 1.0 m); (b) *in situ* split clasts at site 2; (c) fractured bedrock close to the base of the cliff at site 6; (d) breccia below soil level at the base of the cliff at the site of the excavation shown in Figure 7 (scale = 20 cm).

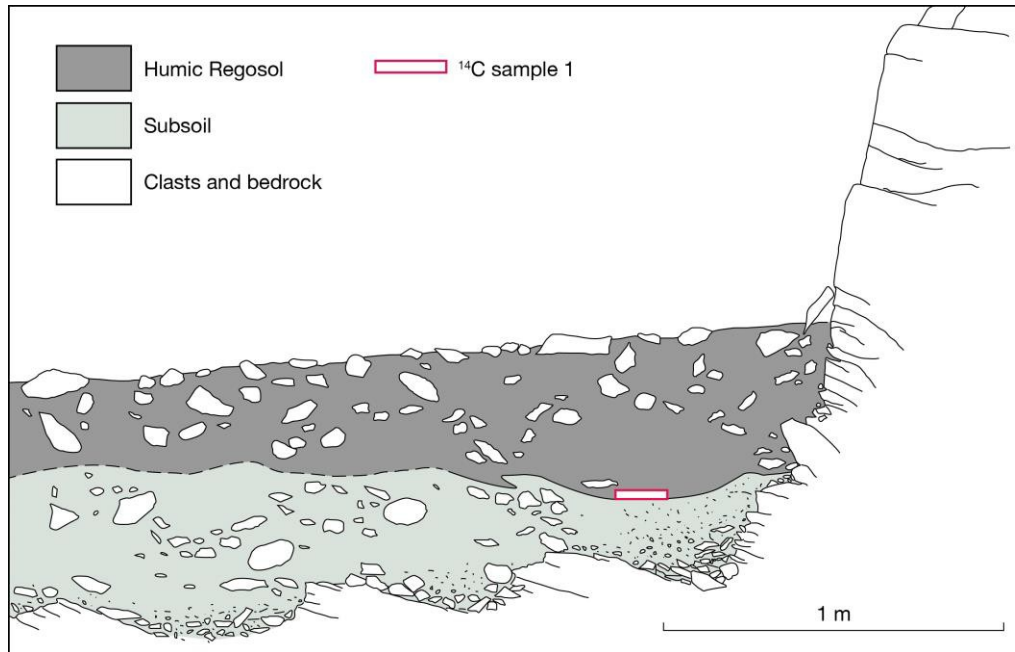


Figure 7. Subsurface characteristics revealed by excavation of the main cryoplanation terrace between sites 5 and 6. Note especially the subsurface bedrock profile and the position of the radiocarbon dating sample at the base of the Humic Regosol.



Figure 8. Standing water at the cliff/tread junction produced by water seeping from the cliff base near site 6 (8/07/2018).

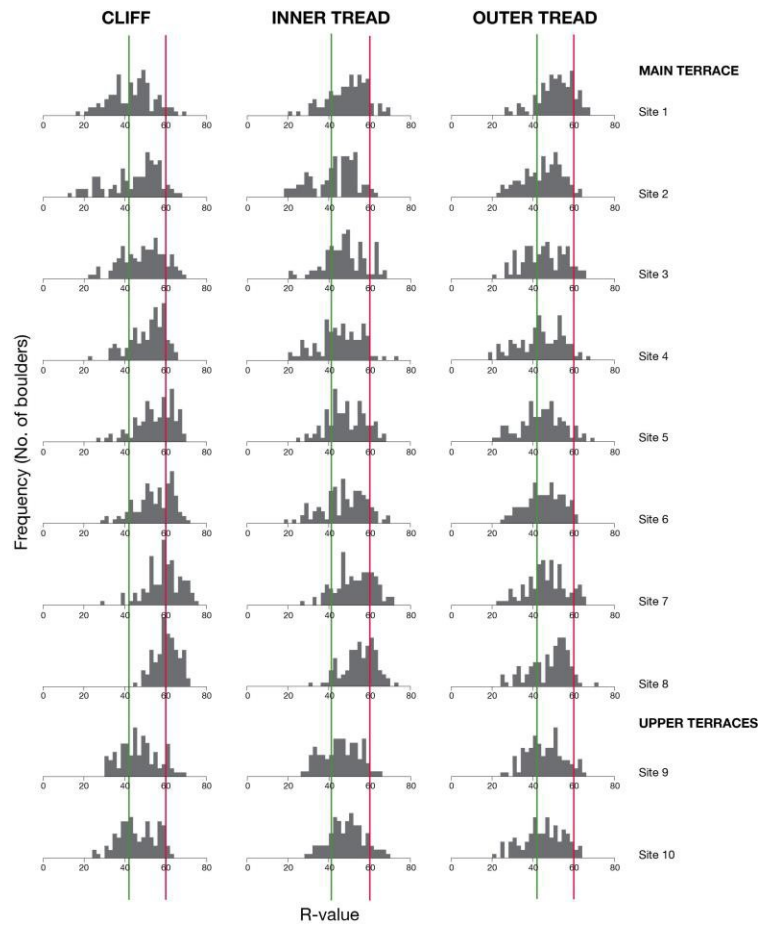


Figure 9. Frequency histograms of R-values for cliffs, and for inner and outer terrace treads, from the 10 sites. Vertical lines represent mean R-values for ‘old’ and ‘young’ control points, respectively.

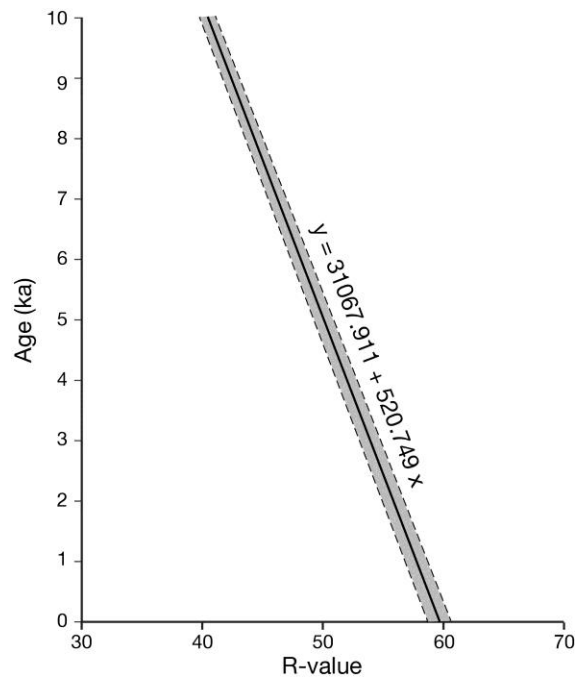


Figure 10. SHD calibration equation and calibration curve with 95 % confidence interval for mylonitised pyroxene-granulite gneiss at Svartkampan.

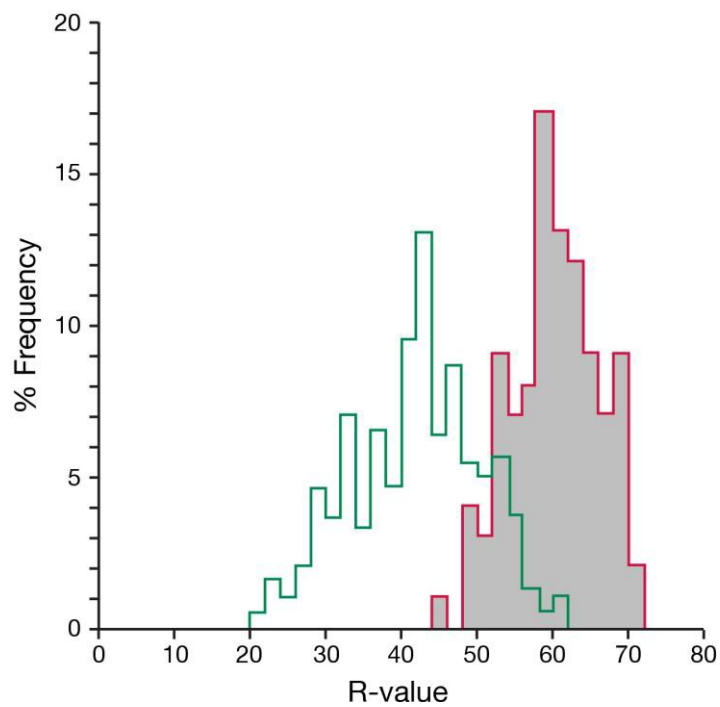


Figure 11. Percentage frequency histograms of R-values for the ‘old’ (9700 ka) and ‘young’ (0 ka; grey shading) control points used in this study. Note that these symmetrical statistical distributions characteristic of single-age surfaces contrast with most of the distributions associated with the cryoplanation terraces in Figure 8.

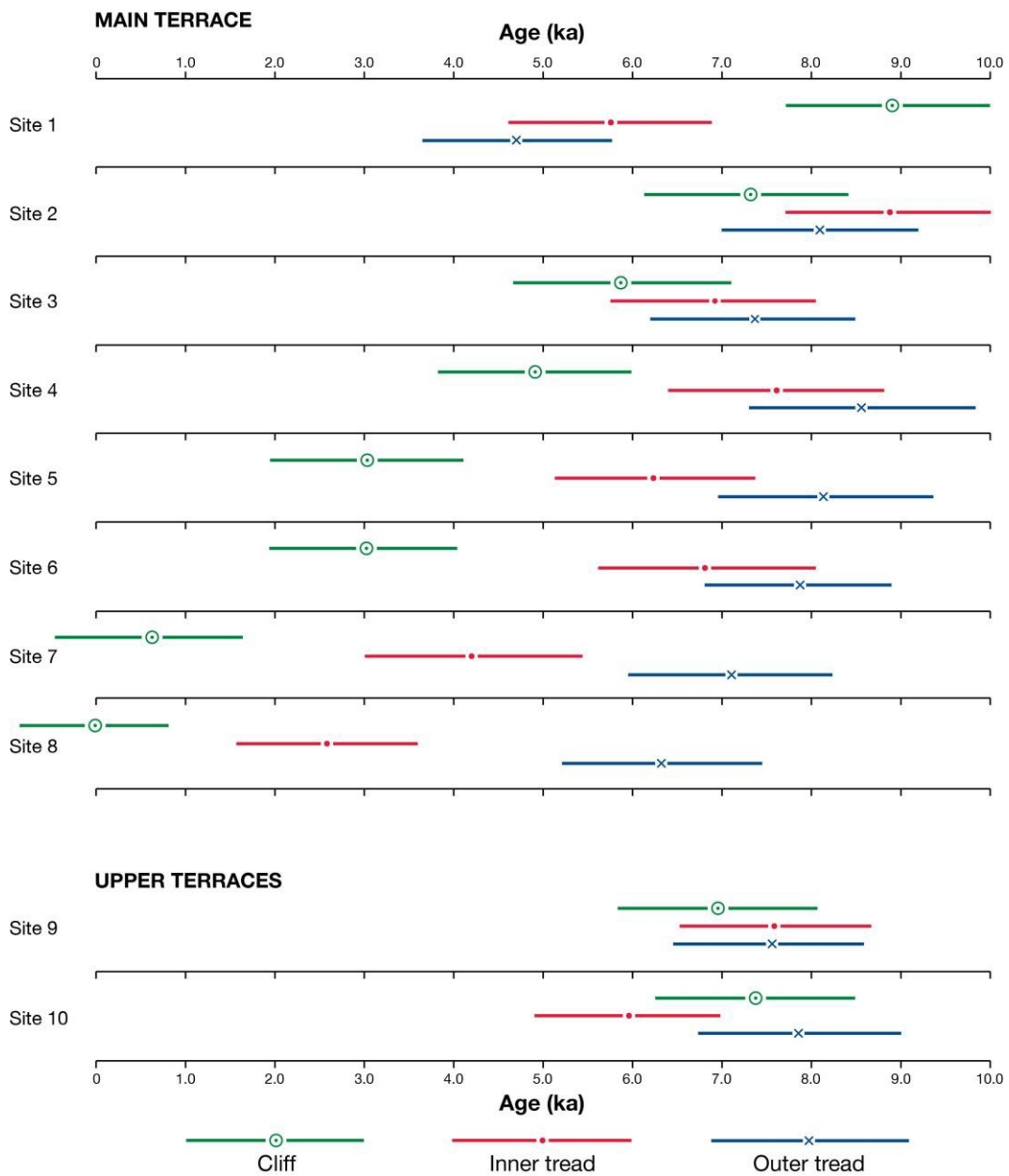


Figure 12. SHD ages for cliffs, inner treads and outer treads at sites from the main terrace (1-8) and the upper terraces (9-10). Horizontal bars are 95 % confidence intervals.

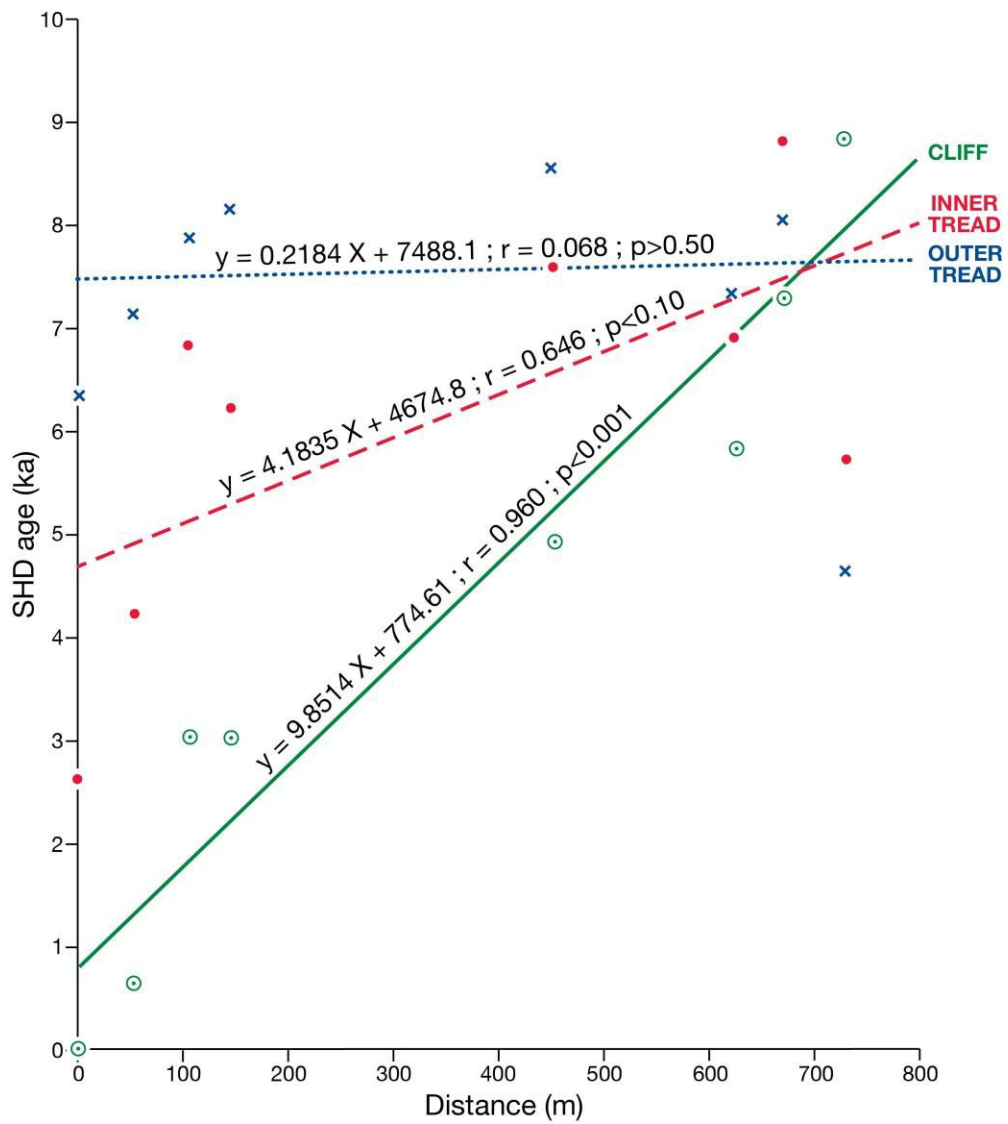


Figure 13. Linear regression analyses and correlation coefficients between SHD age and distance west from site 1 for cliffs, inner treads and outer treads. Note differences in the slope, strength and statistical significance of the relationships (n = 8 for each).

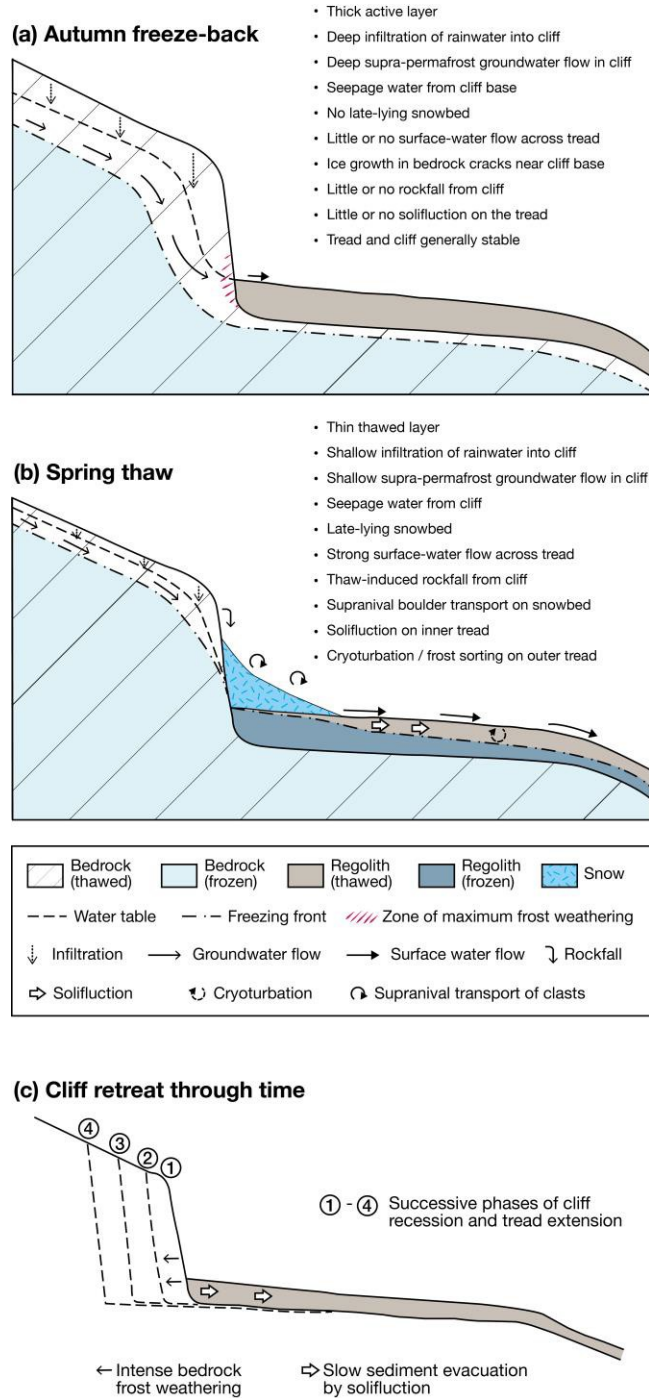


Figure 14. Schematic process-based model of cryoplanation terrace development: processes associated with an active cryoplanation terrace at Svartkampan during (a) autumn freeze-back (prior to the start of freezing) and (b) spring thaw (after thawing has started); (c) the developmental sequence of parallel cliff retreat due primarily to frost weathering of bedrock close to the cliff-tread junction. Note that diagonal lines in the bedrock represent the orientation of the mylonitic layering.

Table 1. Clast characteristics associated with terrace treads and cliffs: angular clasts include angular and very angular roundness categories; edge-rounded clasts include subangular, subrounded and rounded categories; clast size = mean size of the 25 largest clasts in angular or edge rounded categories (\pm 95% confidence interval).

Site No.	Clast roundness (% angular)		Clast size (cm)		Split clasts (%)	Cliff clasts (% angular)
	Inner terrace	Outer terrace	Angular	Edge-rounded		
Main terrace						
1	17	10	79 \pm 8	81 \pm 8	3.8	56
2	43	25	119 \pm 6	63 \pm 8	12.8	81
3	27	19	83 \pm 9	59 \pm 9	5.3	49
4	31	24	120 \pm 12	73 \pm 10	12.4	13
5	27	12	90 \pm 14	75 \pm 8	5.3	87
6	33	13	100 \pm 12	68 \pm 7	5.9	86
7	31	19	95 \pm 8	70 \pm 8	4.0	77
8	77	35	116 \pm 15	68 \pm 8	5.5	97
Upper terraces						
9	14	7	81 \pm 5	90 \pm 8	3.1	82
10	17	5	90 \pm 14	94 \pm 9	4.8	92

Table 2. Schmidt-hammer R-values from cryoplanation terraces (surface boulders) and associated bedrock cliffs: s = standard deviation; CI = 95% confidence interval; n = 100 impacts.

Transect No.	Cliff			Inner terrace			Outer terrace		
	Mean	s	CI	Mean	s	CI	Mean	s	CI
Main terrace									
1	42.59	10.27	2.26	48.66	9.40	2.07	50.66	8.72	1.92
2	45.62	10.47	2.31	42.59	10.36	2.28	44.16	9.40	2.07
3	48.36	10.47	2.31	46.38	9.35	2.06	45.53	9.87	2.18
4	50.22	9.01	1.99	45.05	10.48	2.31	43.19	11.16	2.46
5	53.86	8.91	1.96	47.66	9.16	2.02	43.95	10.55	2.33
6	53.79	9.28	2.05	46.51	10.77	2.37	44.50	9.08	2.00
7	58.45	8.45	1.86	51.54	10.37	2.29	45.96	9.71	2.14
8	59.66	5.62	1.24	54.66	7.84	1.73	47.47	9.55	2.10
Upper terraces									
9	46.52	9.53	2.10	45.10	9.07	2.00	45.24	8.98	1.98
10	45.52	9.23	2.04	48.25	8.55	1.89	44.58	9.66	2.13

Table 3. Schmidt-hammer R-values from local control-point surfaces of known age: s = standard deviation; CI = 95% confidence interval; n = No. of impacts; age of old control points = 9700 years; age of young control points = 0-50 years; M = mylonitised pyroxene-granulite gneiss; G = pyroxene-granulite gneiss.

Lithology	Old control point				Young control point				Source
	Mean	s	CI	n	Mean	s	CI	n	
M	41.03	8.57	0.98	300	59.66	5.62	1.12	100	This study
G1	42.42	9.04	0.94	355	-	-	-	-	This study
G2	38.59	9.16	0.96	350	-	-	-	-	This study
G3	38.04	11.49	1.43	250	57.31	8.25	1.03	250	Matthews et al. (2014)

Table 4. Schmidt-hammer exposure-ages (years) from cryoplanation terraces and associated cliffs: SHD age = mean age \pm 95% confidence intervals of surface boulders or bedrock cliffs; Cs and Cc are the error components used to calculate the confidence intervals (see text). All ages are rounded to the nearest 5 years.

Transect No.	Cliff	Inner terrace			Outer terrace				
		SHD age	Cs	Cc	SHD age	Cs	Cc		
Main terrace									
1	8890 \pm 1185	1065	515	5730 \pm 1115	975	540	4690 \pm 1025	865	545
2	7310 \pm 1210	1085	525	8890 \pm 1195	1075	515	8070 \pm 1105	975	520
3	5885 \pm 1215	1085	535	6915 \pm 1105	970	530	7360 \pm 1150	1025	525
4	4915 \pm 1080	935	545	7610 \pm 1210	1085	525	8575 \pm 1270	1160	515
5	3020 \pm 1080	925	560	6250 \pm 1090	950	535	8180 \pm 1215	1095	520
6	3055 \pm 1115	965	560	6850 \pm 1235	1120	530	7895 \pm 1080	945	520
7	630 \pm 1050	875	580	4230 \pm 1210	1075	550	7135 \pm 1140	1010	530
8	0 \pm 825	585	585	2605 \pm 1000	815	585	6350 \pm 1125	990	535
Upper terraces									
9	6845 \pm 1120	990	530	7580 \pm 1080	940	535	7510 \pm 1070	930	525
10	7365 \pm 1095	960	525	5940 \pm 1040	890	535	7855 \pm 1130	1005	520

Table 5. Radiocarbon dates from the main terrace at Svartkampan. Depth = depth from the terrace surface; distance = distance from the bedrock cliff base.

Lab. No.	Sample No.	Depth (cm)	Distance (cm)	¹⁴ C age (yr BP)	$\delta^{13}\text{C}$ (‰)	Calibrated age range (cal. yr BP; 2 σ)
Beta-501707	1.1	45-43	50	3630 \pm 30	-24.0	4076-3854
Beta-501708	1.2	42-40	60	4130 \pm 30	-24.1	4821-4532
Beta-501709	2.1	60-58	30	3030 \pm 30	-24.8	3345-3084